

BRAIN TUMOR

Targeted inducible delivery of immunoactivating cytokines reprograms glioblastoma microenvironment and inhibits growth in mouse models

Filippo Birocchi^{1,2}, Melania Cusimano^{1†}, Federico Rossari^{1,2†}, Stefano Beretta^{1,2†}, Paola M. V. Rancoita³, Anna Ranghetti¹, Stefano Colombo¹, Barbara Costa⁴, Peter Angel⁴, Francesca Sanvito⁵, Marcella Callea⁵, Rossana Norata⁶, Linda Chaabane⁷, Tamara Canu⁷, Antonello Spinelli⁷, Marco Genua¹, Renato Ostuni^{1,2}, Ivan Merelli^{1,8}, Nadia Coltella^{1*†}, Luigi Naldini^{1,2*†}

Glioblastoma multiforme (GBM) is the most common and lethal brain tumor characterized by a strongly immunosuppressive tumor microenvironment (TME) that represents a barrier also for the development of effective immunotherapies. The possibility to revert this hostile TME by immunoactivating cytokines is hampered by the severe toxicity associated with their systemic administration. Here, we exploited a lentiviral vector-based platform to engineer hematopoietic stem cells *ex vivo* with the aim of releasing, via their tumor-infiltrating monocyte/macrophage progeny, interferon- α (IFN- α) or interleukin-12 (IL-12) at the tumor site with spatial and temporal selectivity. Taking advantage of a syngeneic GBM mouse model, we showed that inducible release of IFN- α within the TME achieved robust tumor inhibition up to eradication and outperformed systemic treatment with the recombinant protein in terms of efficacy, tolerability, and specificity. Single-cell RNA sequencing of the tumor immune infiltrate revealed reprogramming of the immune microenvironment toward a proinflammatory and antitumoral state associated with loss of a macrophage subpopulation shown to be associated with poor prognosis in human GBM. The spatial and temporal control of IL-12 release was critical to overcome an otherwise lethal hematopoietic toxicity while allowing to fully exploit its antitumor activity. Overall, our findings demonstrate a potential therapeutic approach for GBM and set the bases for a recently launched first-in-human clinical trial in patients with GBM.

INTRODUCTION

Tumors coevolve with their microenvironment (TME), shaping it toward an immunosuppressive state, favoring immune escape (1). A paradigmatic example of immunosuppressive tumor is glioblastoma multiforme (GBM), the most aggressive brain tumor. To date, GBM remains a fatal disease with limited benefit of standard therapies, namely, surgical resection, radio- and chemo-therapy with temozolomide (2, 3), and innovative immunotherapies (4–6). The failure of immunotherapies in GBM has been ascribed to the immune distinct site in which these tumors grow, the limited biodistribution of therapeutics from the systemic circulation, and a strongly immunosuppressive TME (7, 8). Targeted delivery of immunoactivating cytokines may surmount these hurdles; however, their controlled expression and tight regulation remain challenging. Gene- and cell-based delivery of cytokines may overcome severe adverse events linked to their systemic administration and enhance safety and efficacy of the treatment (9). Rather than relying on systemic biodistribution,

this strategy aims to spare off-target tissues and reach effective and stable expression only at the disease site without undergoing large fluctuations, thus limiting the risk of adverse events, off-target effects, and desensitization from exposure to excessive dosing. Potential candidates are interferon- α (IFN- α) and interleukin-12 (IL-12), whose therapeutic benefits depend on pleiotropic activities on tumoral, stromal, and immune components of the TME but are undermined by concomitant systemic toxicity (9–12).

To deliver IFN- α at the tumor site, we took advantage of a population of tumor-associated TIE2-expressing monocytes/macrophages (TEMs) and naturally infiltrating the TME. Hematopoietic stem cells (HSCs) were transduced with a lentiviral vector (LV) expressing the cytokine under positive regulation of the *Tie2* enhancer/promoter and negative regulation of HSC-specific microRNAs (miRNAs) recognizing complementary target sequences in the vector (mirT) (13, 14). Transplantation of these engineered HSCs induced TEM-specific release of IFN- α in the TME, favoring immune activation and therapeutic responses in different experimental tumor models (14–17). However, whether this strategy might be effective also in a stringent immunocompetent model of a tumor poorly responsive to immunotherapies such as GBM is unknown. The possibility to tightly control cytokine secretion in a temporal manner and switch it ON and OFF according to disease progression and response remains unavailable.

Exogenously operated transcriptional switches, such as tetracycline-based ones, require distinct transcriptional components under the control of orthogonal promoters, calling for challenging simultaneous delivery of multiple actionable elements (18). Recently, single-component switches, based on the fusion of drug-responsive

¹San Raffaele Telethon Institute for Gene Therapy (SR-Tiget), IRCCS San Raffaele Scientific Institute, 20132 Milan, Italy. ²Vita-Salute San Raffaele University, 20132 Milan, Italy. ³CUSB-University Center for Statistics in the Biomedical Sciences, Vita-Salute San Raffaele University, 20132 Milan, Italy. ⁴Division of Signal Transduction and Growth Control, DKFZ-ZMBH Alliance, German Cancer Research Center (DKFZ), 69120 Heidelberg, Germany. ⁵Pathology Unit, Division of Experimental Oncology, IRCCS San Raffaele Scientific Institute, 20132 Milan, Italy. ⁶GLP Test Facility, San Raffaele Telethon Institute for Gene Therapy (SR-Tiget), IRCCS San Raffaele Scientific Institute, 20132 Milan, Italy. ⁷Experimental Imaging Center, Preclinical Imaging Facility, IRCCS San Raffaele Scientific Institute, 20132 Milan, Italy. ⁸National Research Council, Institute for Biomedical Technologies, 20054 Segrate, Italy.

*Corresponding author. Email: coltella.nadia@hsr.it (N.C.); naldini.luigi@hsr.it (L.N.)

†These authors contributed equally to this work.

destabilizing domains (DDs) to the protein of interest, have been described to control gene expression at the post-translational level (19–21). Whereas the fusion protein is recognized as incorrectly folded and sent to proteasome degradation, it acquires a stable conformation in the presence of a small drug binding the DD.

Here, we assessed the efficacy of DD-fused IFN- α and IL-12 by intratumoral TEM-mediated gene delivery and showed therapeutic effects in a relevant mouse model of GBM (22). Inducible release of IFN- α effectively reprogrammed the GBM TME toward immune activation, sparing peripheral organs. These effects were accompanied by loss of a protumoral gene expression program in tumor-associated macrophages (TAMs) correlating with a worse prognosis in the human disease.

RESULTS

TEM-based IFN- α delivery inhibits tumor growth and prolongs survival in a relevant GBM mouse model

To apply our LV-based IFN- α delivery platform, we took advantage of a syngeneic model of mouse glioma (mGB2) that recapitulates most features of the human tumor (22). Green fluorescent protein (GFP)-marked GBM cells injected in the striatum of mice showed infiltration in surrounding parenchymal regions (fig. S1A). Immunofluorescence staining showed abundant F4/80-IBA1 (ionized calcium-binding adapter molecule 1) double-positive microglia/macrophages within the tumor with amoeboid morphology (fig. S1B). A small fraction of the hematopoietic infiltrate was composed of TEMs, as defined by coimmunostaining for TIE2 and CD45, which were present selectively within the tumor mass and not in the unaffected brain (fig. S1, C and D). Consistent with TIE2 tissue expression, not all TIE2⁺ cells were TEMs, but some of them stained positive for the endothelial marker CD31 and morphologically appeared as endothelial cells (fig. S1E). As expected, the TME was largely composed of myeloid cells and, to a lower extent, lymphoid CD3⁺ cells (fig. S1F). Infiltration of human glioma by TEMs was previously reported (23).

We transplanted lethally irradiated C57Bl/6 mice with HSCs transduced either with Tie2-*Ifna1*-mirT LV (hereafter referred to as “IFN- α ” mice) or with an empty LV [control (“CTRL”) mice] (Fig. 1A). Hematopoietic reconstitution with transplanted cells had a median of about 82% and a vector copy number (VCN) of about 0.6 in the blood cells of IFN- α mice, whereas it was higher in the CTRL (Fig. 1B and fig. S2A). White blood cell (WBC) counts remained significantly lower in IFN- α mice compared to CTRL ($P < 0.0001$) (Fig. 1C), mostly due to lower numbers of lymphocytes (fig. S2, B to D). IFN- α was measurable in the plasma of IFN- α mice (median, 47 pg/ml), whereas it was at or below the detection amount in CTRL mice (Fig. 1C).

To evaluate the antitumor activity of engineered hematopoiesis, we injected 5×10^5 mGB2 cells in the striatum of IFN- α - or CTRL-transplanted mice. Tumor growth was significantly inhibited in IFN- α mice compared to CTRL, as shown by magnetic resonance imaging (MRI) and gross tumor burden measurement ($P = 0.007$) (Fig. 1, D and E). IFN- α concentrations in the plasma of tumor-bearing IFN- α mice at the end of the experiment were comparable to those measured in tumor-free IFN- α mice, indicating that the basal systemic transgene output was independent of the tumor growing in the central nervous system (CNS) (Fig. 1, C and F). We then performed another set of experiments to evaluate survival to tumor challenge while monitoring tumor growth by MRI. Mice belonging to

the IFN- α group survived significantly longer than CTRL ($P = 0.0085$), and a fraction of them cleared the tumor and survived long term (Fig. 1, G and H).

To better assess the role of TEM-mediated IFN- α release within the TME in mediating antitumor response, we tested our gene therapy strategy in another GBM mouse model (GL261) (6), which is not infiltrated by TEMs (fig. S2E). Although transduction efficiency and IFN- α concentration in peripheral blood (PB) were similar or even higher than in the GBM model tested previously, we did not detect any prolonged survival in IFN- α mice compared to CTRL (fig. S2, F to L). Overall, these findings indicate that TEM-based IFN- α gene delivery can effectively delay or even suppress GBM growth, whereas the sole presence of low circulating amounts of IFN- α is not sufficient to elicit antitumor responses.

IFN- α -DHFR shows inducible secretion and is functional in vitro

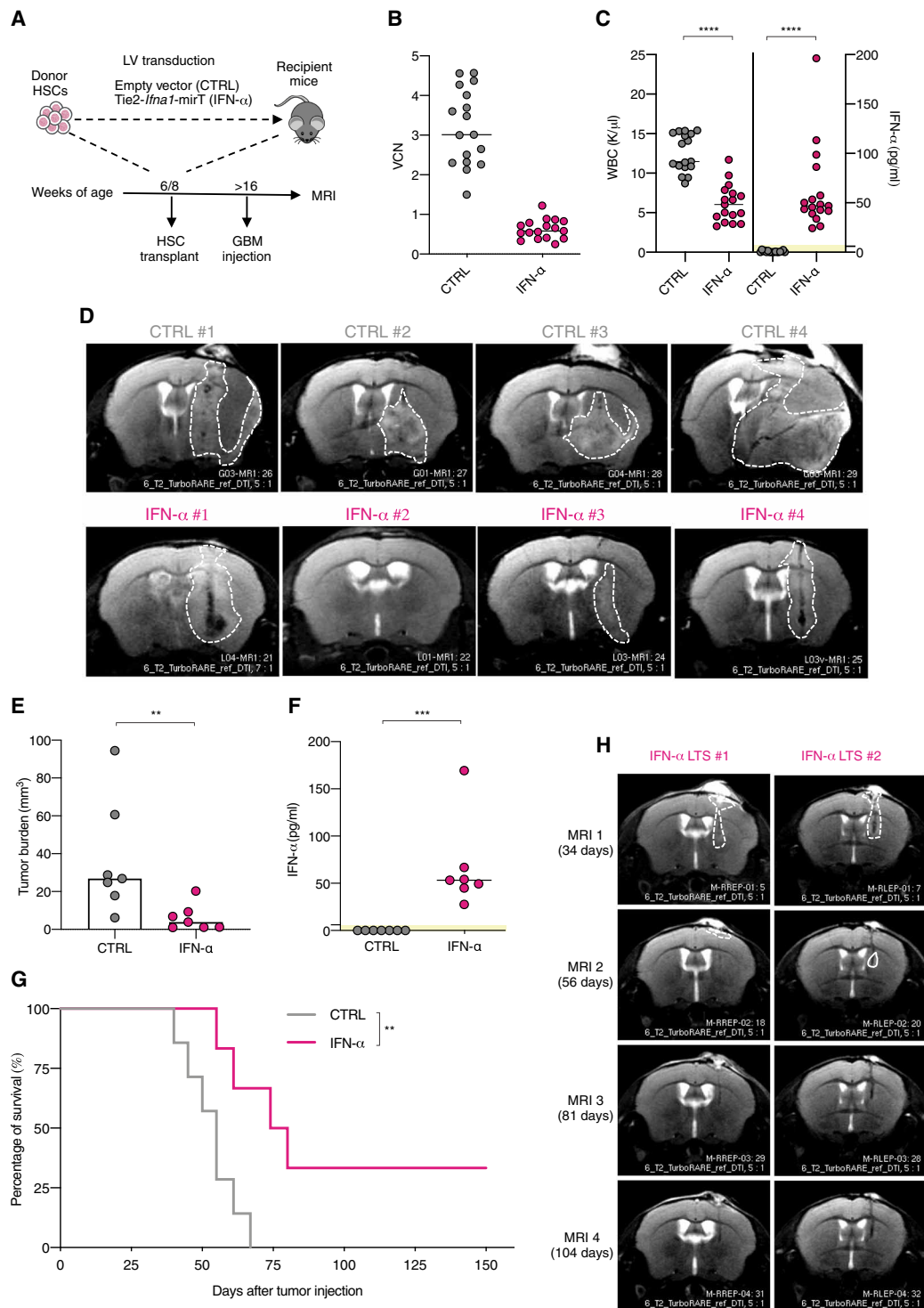
To overcome any potential systemic effect due to basal IFN- α expression, we designed a switchable version of the LV delivery platform. We built an inducible form of IFN- α by fusing the transgene to a mutant DD from *Escherichia coli* dihydrofolate reductase (DHFR), whose stabilizing ligand, trimethoprim (TMP), is a clinically approved drug that crosses the blood-brain barrier (20, 24). We cloned DHFR either at the N or C terminus of mouse *Ifna1* complementary DNA and compared the expression and activity of the fusion proteins with wild-type (wt) IFN- α by LV transduction of TIE2-expressing brain endothelial cells (bEnd.3) (fig. S3, A to C). Fusion of DHFR to the N terminus of IFN- α (DHFR-IFN- α) abolished cytokine secretion in all conditions. On the contrary, fusion to the C terminus (IFN- α -DHFR) resulted in low basal expression at steady state but robust (~12-fold) induction upon TMP administration, although the output was lower than that of wt IFN- α per LV copy (fig. S3D). As DHFR fusion can interfere with binding to the IFN- α receptor, we measured the induction of two IFN-stimulated genes (ISGs; *Irf7* and *Oas1a*) in response to increasing concentrations of wt and IFN- α -DHFR molecules (fig. S3, E and F). Both molecules showed a dose-dependent increase in activity, with IFN- α -DHFR reaching a lower plateau at a higher dose than wt IFN- α , suggesting that the presence of the DHFR moiety may limit binding rate and affinity for the receptor. Because the lower specific activity of IFN- α -DHFR may help suppress basal expression in the OFF state and limit the spreading of the response from a local source in the ON state, we further investigated its application to GBM gene therapy.

IFN- α -DHFR gene therapy inhibits GBM growth in a switch-dependent manner

The TMP-inducible strategy adds an additional level of control to the TEM-cytokine delivery system as it allows to timely regulate the secretion of the cytokine through an ON/OFF switch. Moreover, it allows testing its efficacy in vivo after tumor onset, thus better modeling a therapeutic intervention. To examine the efficacy of inducible IFN- α gene delivery in vivo, we injected mGB2 cells and started TMP treatment of both CTRL and IFN- α -DHFR mice 2 weeks after tumor challenge, when tumor lesions were already detectable by MRI (Fig. 2, A and D). In the OFF state, IFN- α was under the lower limit of quantification (LLOQ) in the plasma of IFN- α -DHFR mice, and WBC counts were comparable in CTRL and IFN- α -DHFR (Fig. 2B). After repeated TMP administrations, IFN- α crossed the LLOQ in the plasma of some mice, and WBC counts were slightly lower in

Fig. 1. Antitumor effects of TEM-based IFN- α gene delivery in GBM.

(A) Schematic representation of the experimental design. HSCs were transduced with an empty LV vector (CTRL) or with Tie2-*Irfn1*-mirT LV vector (IFN- α) and transplanted into lethally irradiated C57Bl/6 mice. After hematopoietic reconstitution, mice were challenged with 5×10^5 mGB2 cells injected orthotopically in the striatum of their brains. Mice were followed by MRI analyses. **(B)** VCN measured in the blood cells of CTRL and IFN- α mice ($n = 17$ per group). **(C)** WBC in the PB of CTRL and IFN- α mice (left) ($****P < 0.0001$, U statistic = 12, Mann-Whitney test) and IFN- α measured in the plasma of the same mice at hematopoietic reconstitution (right) ($****P < 0.0001$, U statistic = 289, Mann-Whitney test, considering that all CTRL values were below the LLOQ; yellow box). **(D)** Representative images of T2-weighted MRI scans of four CTRL and four IFN- α mice 42 days after tumor injection. Dashed lines highlight tumor lesions. **(E)** Tumor burden, calculated by MRI scans, of CTRL and IFN- α mice ($n = 7$ per group) 42 days after tumor injection (median) ($**P = 0.007$, U statistic = 4, Mann-Whitney test). **(F)** IFN- α measured in the plasma of mice by enzyme-linked immunosorbent assay (ELISA) 44 days after tumor injection ($***P = 0.0006$, U statistic = 49, Mann-Whitney test, considering that all CTRL values were below the LLOQ). **(G)** Kaplan-Meier survival curves of mGB2-bearing CTRL ($n = 7$) and IFN- α ($n = 6$) mice ($**P = 0.0085$, $\chi^2 = 6.919$, $df = 1$, log-rank Mantel-Cox test). **(H)** Serial MRI scans of two long-term survivors (LTS) of the IFN- α group. Dashed lines reveal the extent of the tumor lesions.



IFN- α -DHFR compared to CTRL mice (Fig. 2C). Sequential MRIs showed significant inhibition of tumor growth in the IFN- α -DHFR group as confirmed by tumor burden evaluation at 25 days ($P = 0.0102$) and 40 days ($P = 0.0002$) (Fig. 2, D and E). IFN- α -DHFR mice survived longer than CTRL ($P = 0.0014$), with one mouse clearing the tumor and remaining tumor-free even upon TMP withdrawal, when IFN- α in the plasma returned under the LLOQ (Fig. 2, F to I).

We then compared the survival of IFN- α -DHFR mice treated or not with TMP with CTRL (fig. S4A). Whereas IFN- α -DHFR mice treated with TMP displayed prolonged survival ($P = 0.0009$), untreated IFN- α -DHFR mice were undistinguishable from CTRL,

confirming tight control of the switch in the OFF state (fig. S4B). One mouse belonging to the ON group survived long term, cleared the tumor, and overcame tumor rechallenge in the contralateral brain hemisphere even in the absence of TMP, suggesting induction of protective immunity upon the first challenge (fig. S4C).

Overall, these findings indicate that gene delivery of inducible IFN- α inhibits growth up to clearance of already established tumors

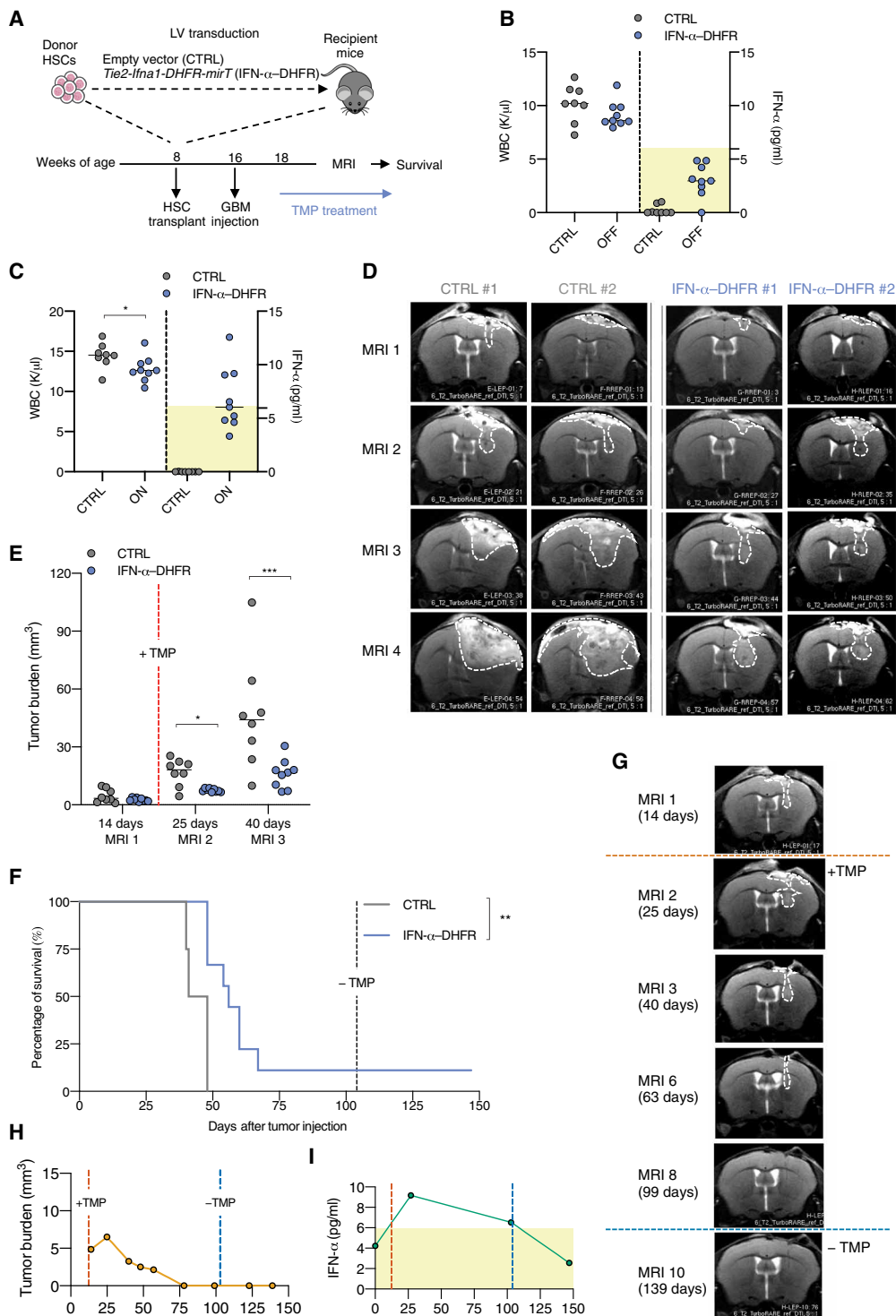


Fig. 2. Inducible TIE2-IFN- α -DHFR gene therapy inhibits GBM growth and prolongs mice survival.

(A) Schematic representation of the experimental design. HSCs were transduced with an empty LV vector (CTRL) or with *Tie2-Iflna1-DHFR-mirT* LV vector (IFN- α -DHFR) and transplanted into lethally irradiated C57Bl/6 mice. After hematopoietic reconstitution mice were challenged with 2.5×10^5 mGB2 cells as in Fig. 1A. Mice were treated with TMP 14 days after tumor challenge by intraperitoneal injection (60 mg/kg, every 48 hours) and followed by MRI. (B) WBC in the PB of CTRL and IFN- α -DHFR mice (left) ($P = 0.1996$, not significant, U statistic = 22, Mann-Whitney test) and IFN- α measured in the plasma of the same mice after hematopoietic reconstitution (right) ($n = 8$ in CTRL and $n = 9$ in IFN- α -DHFR). Concentrations of IFN- α in CTRL and IFN- α -DHFR mice were below the LLOQ of the assay (yellow box). (C) WBC in the PB of CTRL and IFN- α -DHFR mice (left) ($*P = 0.036$, U statistic = 14, Mann-Whitney test), and IFN- α measured in the plasma of the same mice after six doses of TMP (right) ($n = 8$ in CTRL and $n = 9$ in IFN- α -DHFR). (D) Serial, T2-weighted MRI scans of two representative CTRL and IFN- α -DHFR mice (14, 25, 40, and 48 days after mGB2 challenge). Dashed lines highlight tumor lesions. (E) Tumor burden (median), calculated by MRI, of CTRL ($n = 8$), and IFN- α -DHFR ($n = 9$) mice 14 days after tumor injection and before TMP treatment ($P = 0.3704$, not significant, U statistic = 26, Mann-Whitney test). Subsequent MRIs at 25 days ($*P = 0.0102$) and at 40 days ($***P = 0.0002$) after tumor injection. LME model described in Materials and Methods. (F) Kaplan-Meier survival curves of mGB2-bearing CTRL ($n = 8$) and IFN- α -DHFR ($n = 9$) mice ($***P = 0.0014$, $\chi^2 = 10.16$, $df = 1$, log-rank Mantel-Cox test). Dashed line highlights TMP withdrawal. One mouse in the treatment group survived long term in the absence of TMP. (G) Subsequent MRI scans of the long-term survivor, before, during, and after TMP treatment. White dashed lines highlight the extent of tumor lesion during time. (H) Growth kinetics of GBM in the long-term survivor and (I) plasma concentration of IFN- α of the same mouse overtime.

Downloaded from https://www.science.org at Universita Vita Salute - Hospital s. Raffaele on July 14, 2022

and in the near absence of IFN- α in the periphery, demonstrating that TEM-based delivery mostly acts within the tumor.

wt and inducible IFN- α gene therapies similarly improve survival of GBM-bearing mice

To compare the efficacy of wt and inducible IFN- α gene therapy and assess cell dose dependence, we transplanted mice with HSCs

transduced with IFN- α -DHFR, IFN- α , CTRL LV, or a 1:1 mix of IFN- α and CTRL (IFN- α 50%) (fig. S5A). VCN measured in the PB after hematopoietic reconstitution was 1.2 copies per genome for IFN- α -DHFR, 0.7 for IFN- α 100%, and 0.24 for IFN- α 50% (fig. S5B). IFN-mediated effects on the hematopoietic compartment were prevented both in the IFN- α 50% and IFN- α -DHFR (fig. S5, C to F), also consistently with the lower IFN- α concentration measured in

the plasma of these mice (fig. S5G). To possibly maximize the expression of IFN- α -DHFR in the ON state, we used the lactate salt of TMP (TMP-L) at high dose (200 mg/kg) (21). This high dose, however, induced a robust WBC reduction independently from the expression of IFN- α , as shown by a similar decrease induced in tumor-free wt mice (figs. S5, F and H to K). Whereas all treatment groups achieved a similarly prolonged survival compared to CTRL, tumor growth inhibition showed a different kinetic. IFN- α 100% group showed a lower tumor burden at the first MRI, the IFN- α -DHFR group matched the effect of the IFN- α 100% group at the second MRI, whereas the IFN- α 50% group was comparable to CTRL (fig. S5, L to M). This suggests that, although the survival benefit induced by gene therapy may be the result of a threshold IFN- α signaling eventually reached by all the groups, the kinetic of response might depend on the dose of transduced cells transplanted and on the specific activity of the molecule.

IFN- α -DHFR gene therapy shows higher specificity and antitumor activity than systemic IFN- α administration

We then compared efficacy and specificity of our inducible gene delivery strategy with that of systemic delivery of mouse recombinant IFN- α 1 (rIFN- α) at the dose equivalent of a pharmacological treatment in humans (Fig. 3A) (25).

We started rIFN- α or TMP administration 10 days after GBM injection and measured IFN- α in the plasma of mice 4.5 hours after the first dose. Whereas TMP-administered IFN- α -DHFR mice showed barely detectable IFN- α in the plasma (median at the LLOQ of about 5 pg/ml), mice treated with rIFN- α experienced a strong peak (median, 2.4 ng/ml) (Fig. 3B). Subsequent dosing reached higher concentration (median, 5.7 ng/ml) in the plasma of rIFN- α -treated mice, whereas it remained at or below the LLOQ in gene therapy-treated ones (Fig. 3B). At the first MRI, the median tumor burden of both treatment groups appeared slightly lower than that of CTRL. However, at the second MRI, tumor growth was significantly reduced in the IFN- α -DHFR group ($P = 0.041$), whereas mice treated with rIFN- α showed increased tumor burden approaching that of CTRL (Fig. 3C). In another set of experiments, we analyzed the impact of rIFN- α and IFN- α -DHFR treatments on mice survival. We detected a sharp drop in WBC counts 4.5 hours after treatment with rIFN- α , which was almost overlapping with the one induced by the high dose TMP-L treatment in the IFN- α -DHFR group (figs. S6, A and B, and S5, F and H). Although at the first MRI both treatments dampened GBM growth, only IFN- α -DHFR mice survived significantly longer than CTRL ($P = 0.0069$), suggesting that the effect of rIFN- α is lost overtime (fig. S6C and Fig. 3D). Furthermore, rIFN- α mice experienced an early body weight loss during the treatment, as compared to the other groups (fig. S6D).

We then compared on- and off-tumor effects of both strategies. We interrogated a panel comprising representative ISGs and genes encoding for Programmed death-ligand 1 (PD-L1), C-X-C Motif Chemokine Ligand 10 (CXCL10), IL-10, IFN- γ , and IL-12B (fig. S6, E to G). GBM samples showed strong up-regulation of most interrogated genes compared to the respective unaffected brain tissue in all groups (fig. S6F). This up-regulation was highest in the IFN- α -DHFR group, which did not show any change in the unaffected brain tissue, and lowest in the rIFN- α group, in which these genes were highly expressed in both GBM and tumor-free brain tissue (fig. S6, E to G, and table S1). Moreover, when assessing a smaller panel of ISGs in the peripheral organs, we found their strong up-regulation

by rIFN- α in all organs analyzed, whereas IFN- α -DHFR mice showed some induction in the bone marrow, consistent with an expected low basal transgene expression in the ON state in some marrow myeloid cells (Fig. 3I and table S1).

In a second set of experiments, we performed whole transcriptomic analyses [RNA sequencing (RNA-seq)] on unaffected brain samples and sorted tumor cells from all treatment groups. Although we did not detect any differentially expressed gene (DEG) [false discovery rate (FDR) < 0.05] in the comparison between IFN- α -DHFR and control unaffected brain, rIFN- α induced strong up-regulation of several genes involved in IFN response, inflammation, apoptosis, and p53 pathway (Fig. 3, E to G). We then compared the impact of the two IFN- α treatments on GBM cells by gene set enrichment analysis (GSEA) on differential gene expression (DGE) results and found positive enrichment of genes belonging to the hallmark categories of epithelial mesenchymal transition, hypoxia, angiogenesis, glycolysis, inflammatory response, and apoptosis in the gene therapy group (Fig. 3H). These findings suggest that gene-based delivery of IFN- α results in more hypoxic conditions in tumors, which may drive adaptive responses and apoptosis in tumor cells, as compared to recombinant administration, which instead relatively enriches for IFN response categories in the tumor cells.

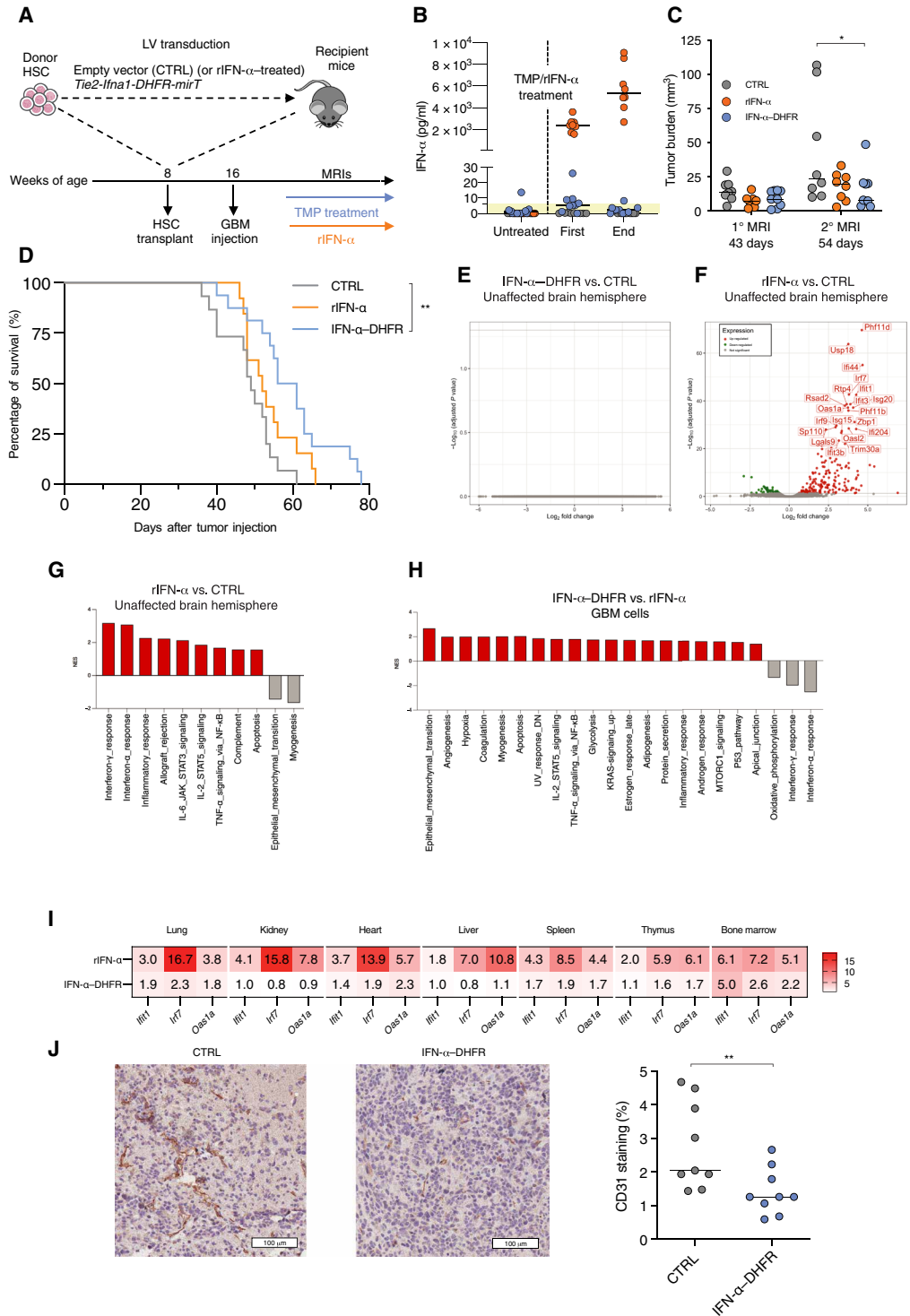
These data provide evidence that targeted IFN- α expression in GBM, as achieved by our gene therapy strategy, not only spares most of the brain and periphery from the effects of the cytokine but also achieves a more robust and durable response within the tumor, which does not depend on higher induction of IFN response in the tumor cells but rather on tumor stroma and/or immune infiltrate.

IFN- α gene therapy targets the GBM TME and promotes immune cell activation

We then investigated the mechanisms through which IFN- α -DHFR gene therapy inhibits GBM growth. Transplanted CTRL and IFN- α -DHFR mice were treated with TMP after mGB2 challenge and histopathological evaluation performed when tumor burden in IFN- α -DHFR was significantly reduced compared to CTRL ($P = 0.0106$) (fig. S7A). CTRL and IFN- α -DHFR tumors showed similar GBM cell morphology and occurrence of apoptotic cells but lower vessel density and fewer cell mitoses in the latter group, as confirmed by quantification of CD31 immunostaining and mitotic counts (Fig. 3J and fig. S7B). These effects are consistent with the up-regulated hypoxic responses observed by RNA-seq in tumor cells and likely contribute to the delayed tumor growth observed in gene therapy-treated mice confirming our previous report of reduced angiogenesis in human glioma xenografts in immunodeficient mice treated with an early version of our platform expressing wt IFN- α (15).

We then investigated the impact of IFN- α gene therapy on the different immune cell populations infiltrating the mGB2 TME. We performed single-cell RNA-seq (scRNA-seq) on sorted donor-derived GBM-infiltrating hematopoietic cells of CTRL, IFN- α -DHFR, and IFN- α gene therapy mice ($n = 3$ per group, mean of 3081 cells per sample retained after quality control filtering; Fig. 4A). Unsupervised graph-based clustering on the overall dataset obtained by integrating all samples and correcting for batch effect identified 19 clusters (Fig. 4B). Cell identities were inferred on the basis of the presence of known lineage-associated genes among the clusters markers (fig. S8A and table S2). Most cells were identified as macrophages (M Φ 1 to 3, proliferating M Φ , and resident-like M Φ), T cells (naïve, CD8, CD4, regulatory T cells (T_{regs}), and proliferating), and, less represented, dendritic

Fig. 3. Comparison between TIE2-IFN- α -DHFR gene therapy and systemic rIFN- α treatment. (A) Schematic representation of the experimental design. See legend of Fig. 2. Mice were treated with TMP 10 days after tumor challenge by intraperitoneal injection. CTRL mice were randomized into two groups and treated with rIFN- α (intraperitoneal injection, 0.05 mg/kg, every 48 hours) or with PBS and followed by MRI. (B) IFN- α measured in the plasma of mice by ELISA before tumor injection (untreated), 4.5 hours after rIFN- α or TMP first treatment, and 4.5 hours after the last dose (end, 56 days). (C) Tumor burden (median), calculated by MRI, of CTRL ($n = 8$), rIFN- α ($n = 8$), and IFN- α -DHFR ($n = 9$) mice 43 and 54 days after tumor injection (post hoc analysis performed only at 54 days: rIFN- α versus CTRL, $P = 0.2611$, not significant; IFN- α -DHFR versus CTRL, $*P = 0.041$; rIFN- α versus IFN- α -DHFR, $P = 0.5$, not significant; LME model described in Materials and Methods). (D) Mice were treated with TMP-L 10 days after tumor challenge by daily intraperitoneal injection (200 mg/kg). CTRL mice were randomized into two groups and treated with rIFN- α as in (A) or with PBS. Kaplan-Meier survival curves of mGB2-bearing CTRL ($n = 15$), rIFN- α ($n = 13$), and IFN- α -DHFR ($n = 16$) mice (rIFN- α versus CTRL, $P = 0.3657$, $\chi^2 = 2.393$, $df = 1$, not significant; IFN- α -DHFR versus CTRL, $**P = 0.0069$, $\chi^2 = 9.294$, $df = 1$; rIFN- α versus IFN- α -DHFR, $P = 0.2487$, $\chi^2 = 3.007$, $df = 1$, not significant; log-rank Mantel-Cox test with Bonferroni correction). (E to H) Three mice per group coming from the experiment in (D) and fig. S6 (A to D) were euthanized 52 days after GBM injection (4.5 hours after the last dose of TMP-L or rIFN- α). RNA-seq was performed on sorted GBM tumor cells and unaffected brain hemisphere samples. Volcano plots showing the results of the differential gene expression (DGE) analysis between (E) IFN- α -DHFR versus CTRL and (F) rIFN- α versus CTRL unaffected brains. Up-regulated genes (FDR < 0.05 and logFC > 0) are highlighted in red, and down-regulated genes (FDR < 0.05 and logFC < 0) are highlighted in green. (G) Preranked GSEA performed on DGE results between rIFN- α and CTRL unaffected brains (Hallmark MSigDB). (H) Preranked GSEA performed on DGE results between IFN- α -DHFR- and rIFN- α -sorted GBM cells (Hallmark MSigDB). NES, normalized enrichment score. (I) In a separate set of experiments, mice were treated as described in (A), and, at the end of the experiment (41 days after tumor injection), organs and tumor samples were collected for RNA expression analyses (CTRL, $n = 5$; rIFN- α , $n = 5$; IFN- α -DHFR, $n = 7$). Heatmap representing the differential expression (fold induction) of three ISGs (*Ifit1*, *Irf7*, and *Oas1a*) in treatment groups over CTRL in different tumor-unrelated organs. Values represent the geometric mean. (J) Representative immunohistochemistry of CD31-stained (brown) sections of GBM samples from CTRL and IFN- α -DHFR mice counterstained with hematoxylin. Dot plot shows CD31 staining (%) per mouse in CTRL and IFN- α -DHFR mice ($n = 9$ per group; $**P = 0.0095$, U statistic = 12, Mann-Whitney test). JAK, Janus kinase; NF- κ B, nuclear factor κ B; STAT, signal transducer and activator of transcription; TNF- α , tumor necrosis factor- α ; UV, ultraviolet; DN, downregulated (up, upregulated); mTORC1, mammalian target of rapamycin complex 1; MYC, MYC Proto-Oncogene.



Downloaded from https://www.science.org at Universita Vita Salute - Hospital s. Raffaele on July 14, 2022

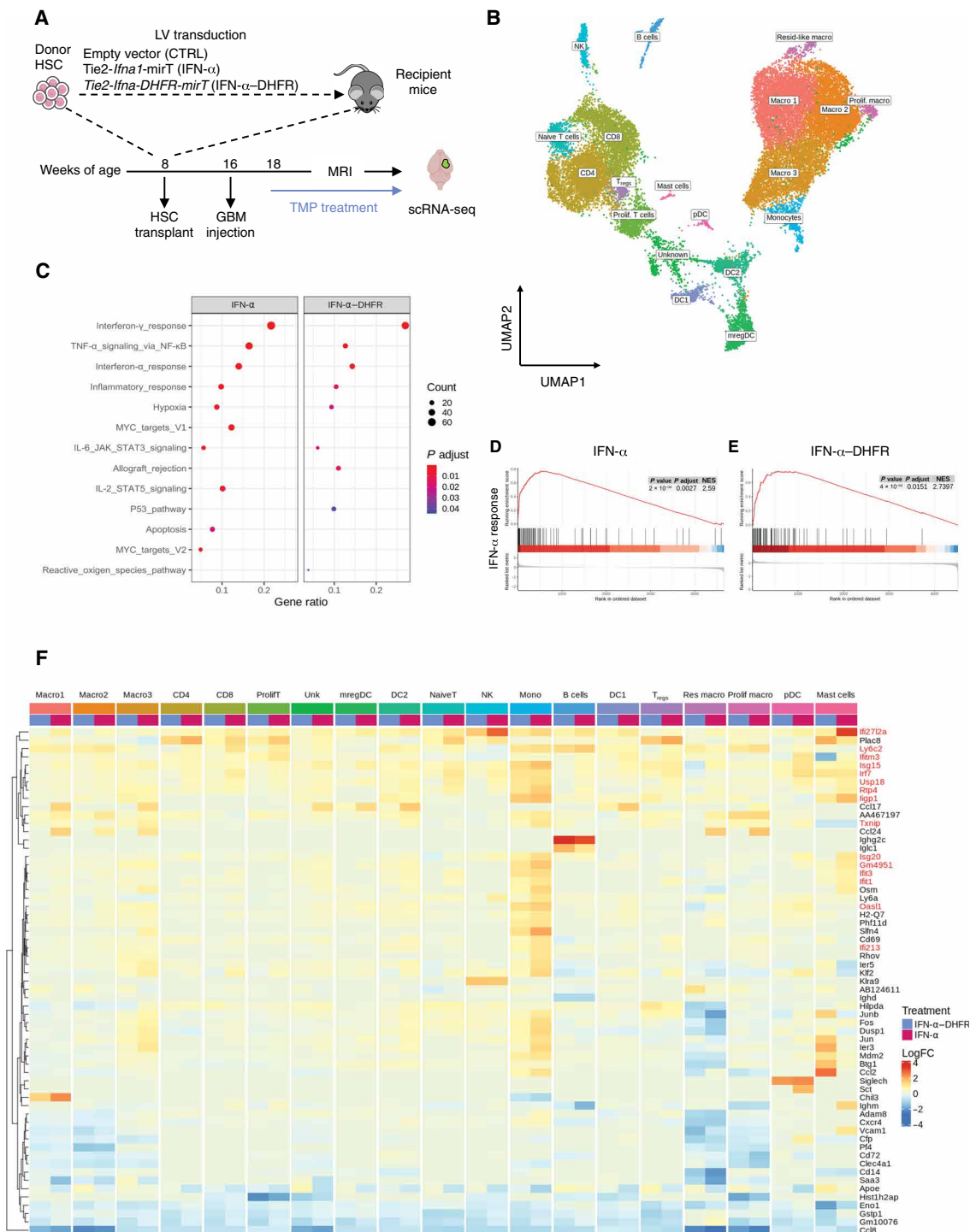


Fig. 4. IFN- α gene therapy broadly elicits an IFN response within the GBM TME and promotes immune cells activation. (A) Schematic representation of the experimental design. Mice were treated with TMP 14 days after tumor challenge (see legend of Fig. 2). At the end of the experiment (41 days after tumor injection), GBM was isolated and dissociated ($n = 3$ per group). Donor-derived CD45.2⁺ hematopoietic cells were sorted, and microdroplet-based scRNA-seq was performed using Chromium Controller (10X Genomics). (B) Uniform manifold approximation and projection (UMAP) plot representing GBM-infiltrating immune cells of the entire dataset obtained by merging all the samples and applying *fastMNN* batch correction. Clusters were obtained with Louvain unsupervised clustering at resolution 0.6. (C) Dot plot showing the results of enrichment analysis on Hallmark categories (from MSigDB) of positive DEGs ($\log_{2}FC > 0$ and $FDR < 10^{-6}$) obtained from the comparison of IFN- α and IFN- α -DHFR groups with CTRL. The x axis represents the gene ratio, the color of the dots represents the adjusted *P* value, and the size of the dots represents the number of enriched genes (count). (D and E) GSEA plots on IFN- α response category from MSigDB performed by considering genes pre-ranked based on $\log_{2}FC$ values resulting from the GDE analysis comparing IFN- α (D) and IFN- α -DHFR (E) groups with CTRL CD45.2⁺ GBM-infiltrating cells. (F) Heatmap showing the DEGs [$abs(\log_{2}FC) > 0$ and $FDR < 0.05$] obtained from the comparison of IFN- α and IFN- α -DHFR groups with CTRL performed in each cluster coming from (B). Genes highlighted in red are IFN-responsive genes.

cells [DC1, DC2, mature DCs enriched in immunoregulatory molecules (mregDC), and plasmacytoid DC (pDC)], as well as other cell types (monocytes, natural killer cells, B cells, and mast cells) (Fig. 4B and fig. S8A). All treatment groups contributed to each cluster to variable extent at this level of analysis (fig. S8B). Enrichment analysis on positive DEGs [log fold change (logFC) > 0 and FDR < 10⁻⁶] between all the cells belonging to both IFN- α gene therapy groups compared to CTRL ones showed an enrichment of hallmark gene sets belonging to IFN- α response, as well as proinflammatory response pathways [such as tumor necrosis factor- α (TNF- α) signaling via nuclear factor κ B and IFN- γ] and hypoxia (Fig. 4C). GSEA on genes preranked on the basis of logFC confirmed positive up-regulation of the IFN- α hallmark category (Fig. 4, D and E). These findings further attest functional IFN- α delivery to the tumor immune infiltrate even in its inducible form. When considering DEGs between treatments and CTRL in each cluster, we found the up-regulation of several ISGs throughout most cell types, with the strongest induction in monocytes (Fig. 4F) and the highest expression in monocytes and DC2 (fig. S8C). These findings are consistent with the expected targeted expression of the TIE2-driven cassette in monocytes, which also showed the largest set of DEGs among all the other clusters. *Ccl8* was the most down-regulated gene across multiple cell types, especially in macrophages, which also showed the down-regulation of several other genes, including *Pf4*, *Clec4a1*, and *Cd72* (Fig. 4F).

We further characterized the changes induced by IFN- α gene therapy in the most represented immune populations by subclustering and reanalyzing separately T cells, DCs, and monocytes/macrophages (Mo/M Φ). Unsupervised clustering of T cells identified eight clusters, of which three comprised CD4⁺ cells and two CD8⁺ ones, whereas the remaining were identified as naïve, regulatory, and proliferating T cells (Fig. 5A, fig. S9A, and table S3). Although all groups contributed to each cluster, the contribution from IFN- α and IFN- α -DHFR was enriched for cluster 7 (CD4_3, enriched in *Ifitm1,2,3*, *Lgals1*, and glycolytic genes such as *Pgk1*, *Hk2*, and *Eno1*) and cluster 4 (CD8_2, enriched in *Ly6c2*, *Ccl5*, *Gzmk*, and *Irf7*) (fig. S9B and table S3). GSEA on DGE results, comparing both IFN- α and IFN- α -DHFR with CTRL T cells, showed a negative enrichment of T cell exhaustion genes in gene therapy groups (Fig. 5B) (26). Flow cytometry analyses confirmed these data at the protein level, showing reduced percentage of cytotoxic CD8⁺ T cells coexpressing the exhaustion markers Programmed cell death protein 1 (PD-1) and Lymphocyte-activation gene 3 (LAG3) in the tumors of IFN- α -DHFR mice compared to CTRL (Fig. 5C). These data suggest that IFN- α gene therapy supports T cell activation and limits their exhaustion. Although B cells accounted for a small fraction of the immune infiltrate, we observed that IFN- α induced immunoglobulin switch from immunoglobulin M (IgM) in the CTRL to IgG in the treatment groups (fig. S9C) (27).

IFN- α gene therapy also affected dendritic cells. Unsupervised clustering identified four populations: pDC, DC1, DC2, and the recently described mregDC (Fig. 5D, fig. S9D, and table S4) (28). GSEA performed on DGE results, between IFN- α and IFN- α -DHFR compared to CTRL DCs, showed positive enrichment of genes induced upon in vitro lipopolysaccharide (LPS) stimulation of DCs and negative enrichment of genes involved in oxidative phosphorylation, in the gene therapy groups, suggesting activation of tumor-infiltrating DCs (Fig. 5, E and F) (29).

Together, these data confirm broad activation of innate and adaptive immune cells of the GBM TME by IFN- α gene therapy, both with the wt and inducible molecule.

IFN- α gene therapy reprograms GBM TAMs toward a proinflammatory phenotype, suppressing a gene expression signature associated with poor prognosis in the human disease

We then evaluated the impact of IFN- α gene therapy on reclustered Mo/M Φ (Fig. 6A). Enrichment analysis performed on positive DEGs (logFC > 0 and FDR < 10⁻⁶) between the two IFN- α gene therapy strategies compared to CTRL showed up-regulation of genes belonging to IFN- α , IFN- γ , and TNF- α signaling (fig. S10A). Among the most down-regulated genes in the gene therapy groups were *Ccl8*, *Pf4*, *Ccl7*, *Selenop*, *Clec4a1*, *Cd72*, *Cd81*, *Eno1*, *Mrc1*, and *Msr1* (Fig. 6B and table S5). A similar gene combination was recently shown to be down-regulated in CNS-associated macrophages upon neuroinflammation (30, 31). Moreover, several of these genes were found down-regulated in TAMs of other tumor models upon genetic knock-out of *Trem2* or *Dab2*, which suppressed TAM protumoral or prometastatic activity (32, 33). This suggests that IFN- α gene therapy phenocopies, at least in part, the genetic knockout of emerging therapeutic targets in a GBM model. GSEA on DGE results, between IFN- α and IFN- α -DHFR compared to CTRL Mo/M Φ , performed using published signatures of murine macrophages stimulated in vitro with proinflammatory (LPS + IFN- γ) or immune modulatory (IL-4) stimuli, showed positive enrichment of M1 genes and negative enrichment of M2 genes in gene therapy-treated groups (fig. S10B) (34).

Unsupervised clustering of GBM-infiltrating Mo/M Φ revealed high heterogeneity with the identification of 11 clusters (Fig. 6A). Some of these clusters could be assigned to specific differentiation stages, functional or polarization states based on marker gene expression: cluster 10, nonclassical monocytes (*Pglyrp1*, *Ace*, *Adgre4*, and *Ear2*); cluster 7, classical monocytes (*Plac8*, *S100a4*, *Ms4a4c*, *Ifitm6*, *Ly6c2*, and *Ccr2*); cluster 9, proliferating monocytes/macrophages (*Stmn1*, *Pclaf*, *Top2a*, and *Birc5*); and cluster 5, macrophages with features of alternative activation (*Chil3*, *Arg1*, and *Mmp12*). Clusters 4 and 1 expressed markers of microglia (*Tmem119*, *Cx3cr1*, *Itgam*, *P2ry12*, and *Olfml3*), suggesting acquisition of microglia-like features by some donor-derived cells in the brain of transplanted mice. Clusters 8, 3, and 0 could not be univocally assigned, possibly reflecting a continuum of states from undifferentiated monocytes/macrophages toward more defined phenotypes (Fig. 6, A, C, and D; fig. S10C; and table S6). Some clusters showed skewed contribution per treatment. Cluster 2 showed higher contribution from the IFN- α gene therapy groups and had features of proinflammatory macrophages (*Dusp1*, *Socs3*, *Il1b*, and *Tnf*). Cluster 6, on the contrary, showed near exclusive contribution from CTRL cells (Fig. 6, C to E; fig. S10C; and table S6). Moreover, marker genes of cluster 6 comprised nearly all the genes listed above that were prominently down-regulated in the IFN- α gene therapy groups (Fig. 6B, fig. S10D, and table S6), highlighting a gene expression program enriched in protumoral/immunosuppressive features and sensitive to IFN- α gene therapy. Because hypoxia is a major feature of human GBM and it is known to promote recruitment and protumoral function of TAMs (35), we interrogated our Mo/M Φ dataset with a published hypoxia gene signature and found that cluster 6 displayed the highest expression of hypoxia-associated genes among a broader population also comprising cells of clusters 5, 3, and 0 (fig. S10, E and F).

Pseudotime and velocity analyses on Mo/M Φ highlighted two alternative main trajectories between treatment and control tumors. In CTRL GBM, a directional flow emerged from cluster 7 monocytes toward intermediate/differentiated macrophages of cluster 3. Instead,

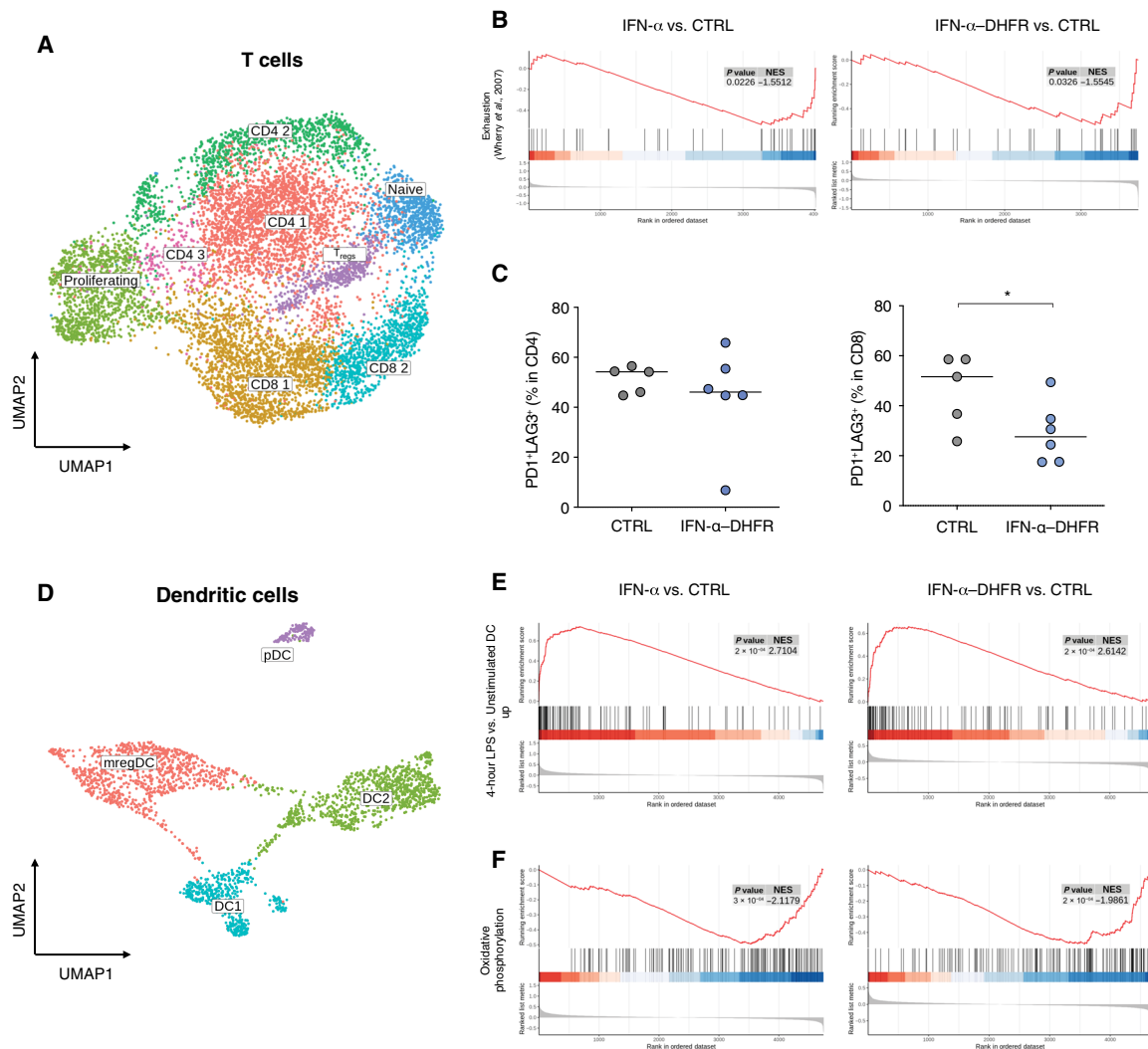


Fig. 5. Effects of IFN- α gene therapy on tumor-infiltrating T cells and DCs. (A) UMAP plot representing the subset of T cells obtained by merging all the samples and applying *fastMNN* batch correction. Clusters were obtained with Louvain unsupervised clustering at resolution 0.6. (B) GSEA plot on published T cell exhaustion signature (26) performed by considering genes preranked on the basis of logFC values resulting from the DGE analysis comparing IFN- α and IFN- α -DHFR with CTRL T cells. (C) Flow cytometry analyses of tumor infiltrating CD4⁺ (left) and CD8⁺ (right) T cells expressing PD-1 and LAG3 markers (CD4⁺, $P = 0.7013$, not significant, U statistic = 12.5; CD8⁺, $*P = 0.0498$, U statistic = 4, Mann-Whitney test). (D) UMAP plot representing the subset of DCs obtained by merging all the samples and applying *fastMNN* batch correction. Clusters were obtained with Louvain unsupervised clustering at resolution 0.1. (E) GSEA plot of published signatures of DCs stimulated with LPS (4-hour LPS versus unstimulated DC up-regulated, GSE14000) and (F) oxidative phosphorylation (Hallmark gene set) performed by considering genes preranked on the basis of logFC values resulting from the DGE analysis comparing IFN- α and IFN- α -DHFR groups with CTRL DCs.

in IFN- α and IFN- α -DHFR GBMs, the major flow emerging from monocytes pointed toward TAMs of the treatment-enhanced cluster 2, suggesting IFN- α -induced polarization toward proinflammatory features (Fig. 7, A and B). These analyses suggest a dynamic TME with high plasticity at the level of blood-derived tumor monocytes, consistent with the finding that IFN- α response is prevalent in cluster 7 and partially in cluster 2 (Fig. 7C).

To investigate whether IFN- α expression by TEMs can affect their ability to infiltrate GBM and locally proliferate or change their polarization status, we quantified their abundance in CTRL, IFN- α , and IFN- α -DHFR GBMs by immunofluorescence staining of tumor sections. We observed a consistent and significant reduction in TEMs in both IFN groups compared to CTRL (IFN- α , $P = 0.0002$; IFN- α -DHFR, $P < 0.0001$) (fig. S10G). Because TEMs are a known

protumoral Mo/M Φ subset, this finding supports the IFN-induced TAM reprogramming uncovered by scRNA-seq.

To study whether the contribution of adaptive immunity was necessary to dampen GBM growth and increase mice survival, we monitored the effect of IFN- α gene therapy in immunocompromised Rag2^{-/-} γ chain^{-/-} mice injected with mGB2 cells (fig. S11A). These mice completely lack the lymphoid compartment while retaining the myeloid one (36). PB analyses at hematopoietic reconstitution showed reduced WBC counts in IFN- α mice compared to CTRL and similar amounts of IFN- α in the plasma as in immunocompetent mice (fig. S11, B and C). IFN- α gene therapy did not significantly affect tumor burden compared to CTRL ($P = 0.115$); however, it prolonged survival ($P = 0.0284$) (fig. S11, D and E). These findings support the contention that some myeloid cells within the TME promote

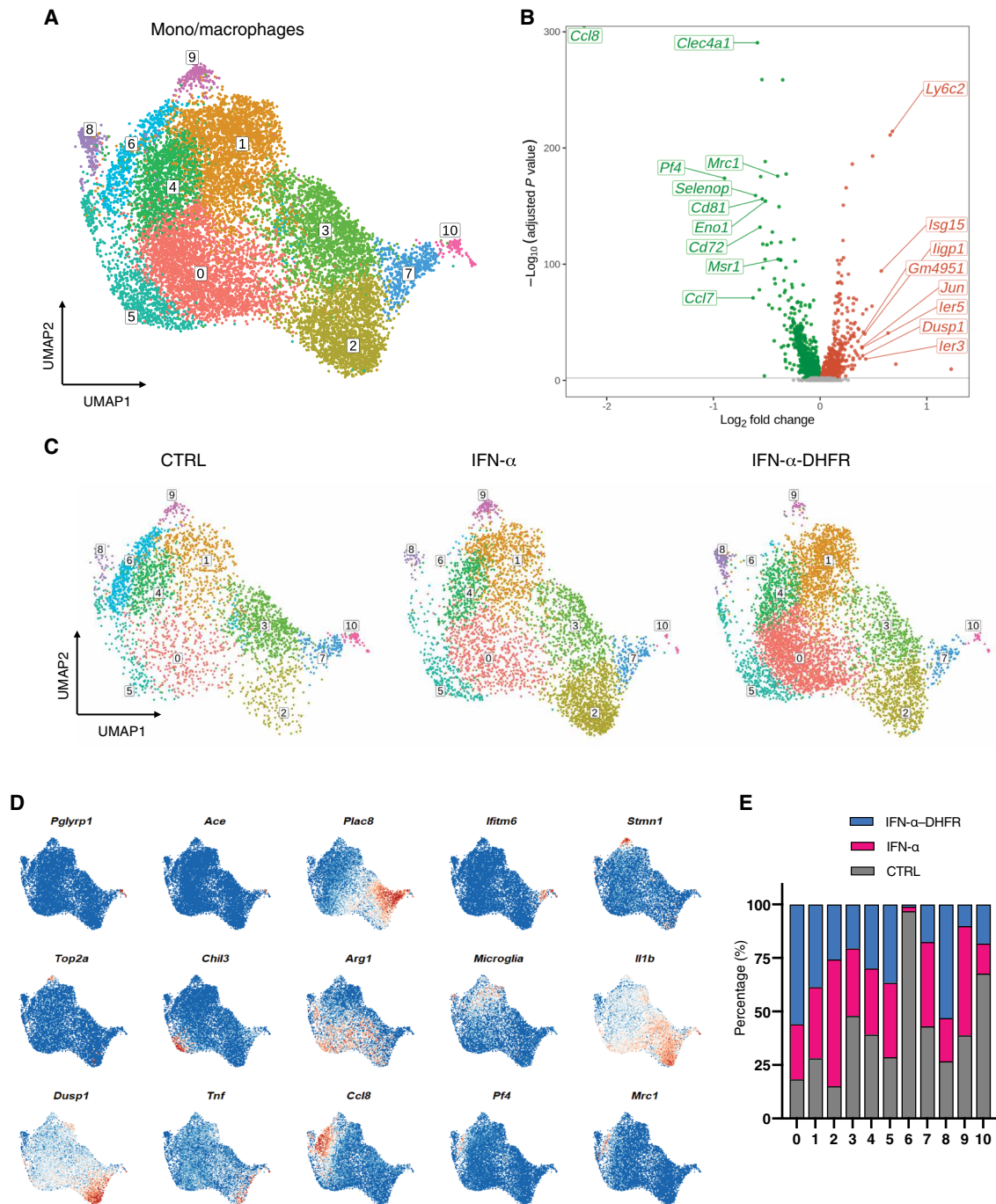


Fig. 6. IFN- α gene therapy reprograms GBM TAMs toward immune activation. (A) UMAP plot representing the subset of tumor-infiltrating CD45.2⁺ Mo/M Φ obtained by merging all the samples and applying *fastMNN* batch correction. Clusters were obtained with Louvain unsupervised clustering at resolution 0.6. (B) Volcano plot showing significant down-regulated (green) and up-regulated (red) genes (adjusted *P* value < 0.01) in Mo/M Φ coming from gene therapy-treated mice (IFN- α and IFN- α -DHFR) compared to CTRL. (C) UMAP plot showed in (A) split by group. (D) UMAP plots showing the average expression of selected genes and signatures characterizing the clusters of UMAP plot showed in (A). (E) Relative contribution of the different groups to each cluster of the UMAP plot showed in (A). The percentage of contribution is normalized on the number of cells of each sample.

tumor growth and that this activity is counteracted by their reprogramming induced by IFN- α gene therapy, together with IFN- α -mediated angiogenic inhibition.

To investigate the potential clinical role of the IFN- α -down-regulated genes highlighted in cluster 6, we defined a 10-gene signature

from the top marker genes (based on logFC) of this cluster (Fig. 7D) and evaluated its association with clinical outcome in The Cancer Genome Atlas (TCGA, Cell 2013) GBM cohort (*n* = 154). High expression of a score defined as the sum of the standardized intensities of the genes of this signature was associated with significantly reduced

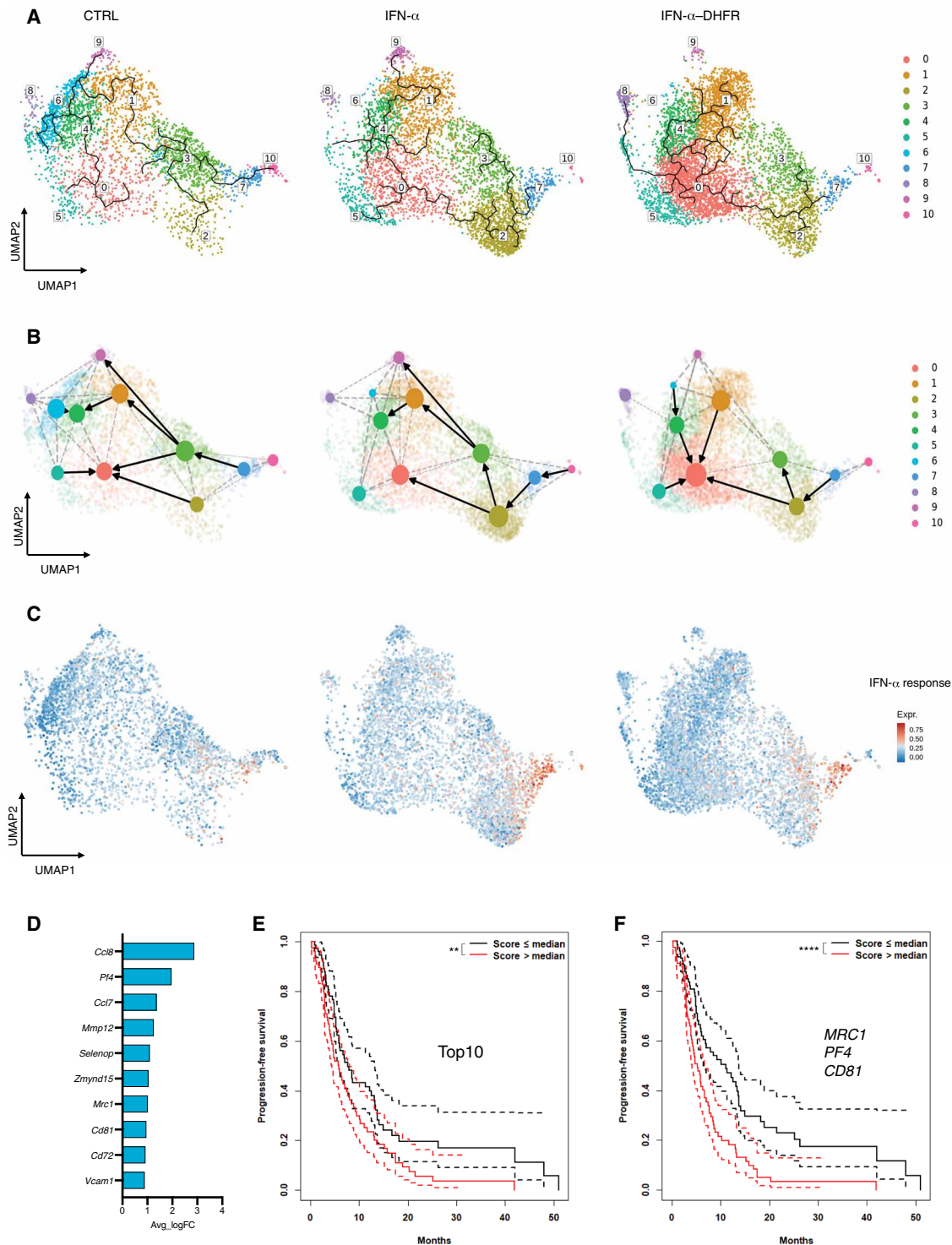


Fig. 7. A group of genes in cluster 6 predicts worse PFS in human GBM. (A) UMAP plot of Mo/M Φ with clusters as in Fig. 6A with Monocle3 trajectory graphs of pseudo-time built on Seurat embedding and split by group. **(B)** RNA velocity trajectories computed with scVelo and represented with PAGA velocity graph projected onto Mo/M Φ UMAP plot. Arrows indicate inferred RNA velocity direction among clusters. **(C)** UMAP plot of Mo/M Φ cells split by group, showing the average expression of genes from the Hallmark IFN- α response category from MSigDB. **(D)** Top 10 marker genes (by logFC values) of cluster 6 of Mo/M Φ dataset. **(E and F)** Kaplan-Meier curves of the PFS with respect to the scores categorized with the corresponding median value obtained from the TCGA GBM (Cell 2013) dataset (for the definition of the scores see statistics in Materials and Methods). In (F), the genes reported are the ones selected by the Cox's proportional hazards model with Lasso penalty. In both (E) and (F), log-rank Mantel-Cox test was used for comparing the two curves [(E) ** $P=0.0097$, $\chi^2=6.7$, $df=1$; (F) **** $P<0.0001$, $\chi^2=16.2$, $df=1$, log-rank Mantel-Cox test].

progression-free survival (PFS; $P = 0.0097$) (Fig. 7E). Cox's regression with Lasso penalty analysis identified a score based on three genes (*PF4*, *MRC1*, and *CD81*) driving the negative prediction of GBM PFS ($P < 0.0001$) (Fig. 7F).

Collectively, these data suggest that IFN- α gene therapy strategies reprogram a heterogeneous GBM TAM repertoire with protumoral features toward immune activation. The absence of a unique gene expression program associated with poorer prognosis in human GBM in the IFN- α and IFN- α -DHFR groups supports the translational value of TEM-based gene therapy.

Inducible delivery of IL-12 overcomes its hematopoietic toxicity and prolongs mice survival

We then evaluated the anticancer potential of another immunostimulatory cytokine, IL-12 taking advantage of our cell and gene therapy approach. We cloned a single-chain IL-12 (*sc-IL12*) transgene encoding the p35 and p40 subunits in the Tie2-mirT LV. Although the LV design limits cytokine exposure in the BM, all mice transplanted with HSCs transduced with the constitutive transgene died within 30 days after transplant, highlighting a strong toxicity of the molecule in the hematopoietic recovery phase (Fig. 8A). We, therefore, applied the DHFR platform previously described for IFN- α . On the basis of in vitro inducibility, we selected the N-terminal fusion for high IL-12 secretion upon TMP administration and low basal expression in its absence. This fusion molecule induced IFN- γ secretion by splenocytes with similar dose dependence as wt IL-12 although reaching a slightly lower plateau (Fig. 8, B and C). We then evaluated the antitumor activity of the inducible DHFR-IL-12 in the GBM model. The toxicity observed with Tie2-*IL12*-mirT LV was fully overcome when transplanting the inducible version in the OFF state, allowing complete hematopoietic reconstitution with a similar range of VCN as that observed for the IFN- α -DHFR (Fig. 8, D and E). We then compared the antitumor effects of inducible IFN- α and IL-12 gene therapies. Both cytokines became barely detectable in the circulation upon TMP treatment (Fig. 8, F and G). IL-12-transplanted mice did not experience hematopoietic toxicity even upon TMP induction (Fig. 8E). Both cytokine gene therapies significantly prolonged survival as compared to CTRL (IFN- α -DHFR, $P = 0.0036$; DHFR-IL-12, $P = 0.0432$), although only IFN- α -DHFR resulted in significantly reduced tumor volume at the second MRI ($P = 0.0183$) (Fig. 8, H and I). One mouse belonging to the DHFR-IL-12 group survived long term, cleared the original tumor, and resisted tumor rechallenge (Fig. 8, I and J). These data confirm the portability of our inducible cell and gene therapy strategy to antitumoral payloads and demonstrate its potential to unleash the therapeutic power of otherwise toxic immunostimulatory cytokines.

DISCUSSION

Here, we show inhibition up to eradication of a syngeneic GBM mouse model closely resembling the human disease (22) by an inducible gene-based platform for targeted delivery of immunostimulating cytokines to the tumor site in a tight space- and time-controlled manner. Selective IFN- α delivery inhibited angiogenesis and induced pervasive remodeling of the immune cells infiltrating the GBM TME, with decreased exhaustion of T cells and reprogramming of the recruited TAMs toward a proinflammatory state while suppressing a protumoral signature comprising genes associated with immune suppression, tumor progression, and metastasis (32, 37),

and here shown to have negative prognostic value in the human disease. A possible source of this reprogramming was ascribed to monocytes, conceivably recruited from the bloodstream, which may sense local signaling cues and mature correspondingly into different TAM subsets. Accordingly, the frequency of TEMs was lower in GBM of gene therapy-treated than CTRL mice, possibly reflecting the occurrence of an autocrine loop in IFN- α -producing cells that shift the balance from protumoral to antitumoral features, and may also prevent excessive transgenic IFN- α release by negative feedback. Follow-up studies investigating the mechanisms underlying proneoplastic effects of the gene expression program characterizing TAMs of cluster 6 and suppressed by IFN- α may further validate our therapeutic strategy and unravel potential therapeutic targets in the TME.

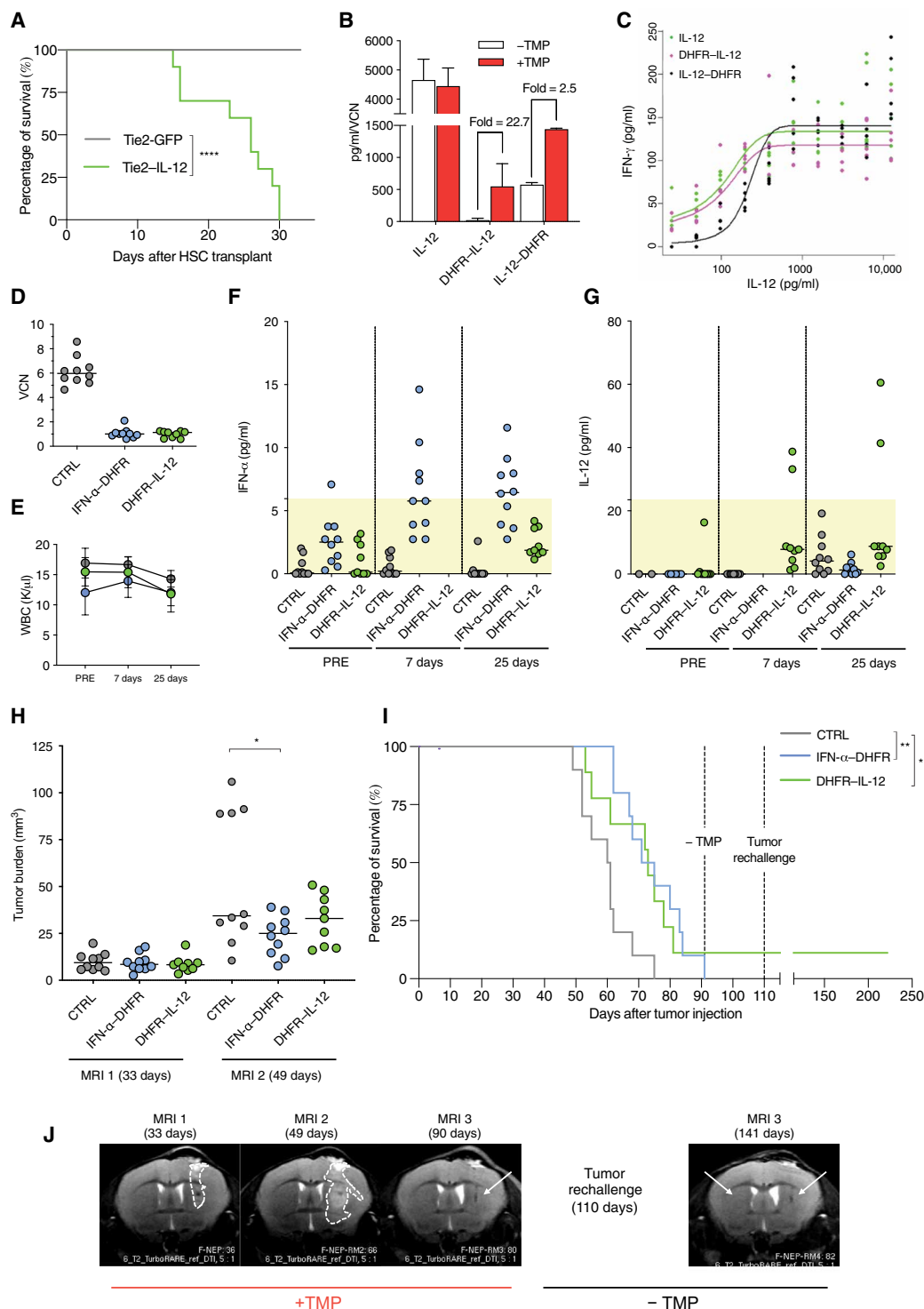
Although tumor clearance was observed only in a small fraction of mice, its occurrence is consistent with the potential of our strategy to induce a protective immune response directed against tumor-associated antigens observed in other tumor models (17). Stochastic variation in the individual T cell receptor repertoire, the extent of T cells recovery after conditioning, or treatment-induced perturbation (as upon high dose TMP-L) may determine whether emergence of adaptive immunity leads to tumor eradication or not, as it is often observed when testing immunotherapies on fast-growing tumors (6). Because our gene therapy improved survival also in immunocompromised mice, which lack the lymphoid compartment, its antitumor effects must also derive from the myeloid cell reprogramming per se with associated inhibition of angiogenesis. Up-regulation of ISGs was widespread across the tumor immune infiltrate and associated with enhanced activation features, such as DC maturation, reduced T cells exhaustion, B cell immunoglobulin class switching, and TAM proinflammatory polarization. These readouts of immune cell activation in the TME are reported as predictors and effectors of antitumor responses in several tumors and upon different therapeutic strategies in experimental models and in the clinic (38–41).

The antitumor activity achieved by IFN- α -induced TME reprogramming might be further enhanced by combination with other immunotherapeutic agents such as checkpoint blockers and chimeric antigen receptor T cells, as we previously reported in a B cell acute lymphoblastic leukemia model (17). Clinical translation of our strategy using wt IFN- α is now under investigation in a dose-escalating phase 1/2a clinical trial performed in patients with poor-prognosis GBM (NCT03866109, clinicaltrials.gov) and will provide the first-in-human validation of the safety and potential efficacy of this versatile and innovative platform. Because our IFN- α gene therapy strategy similarly prolonged mice survival when administering only a fraction of transduced HSCs, we envision that efficacy can be achieved upon reaching a low threshold dose in the tumor.

Specific intratumoral release of proinflammatory cytokines with our inducible delivery platform was superior to standard systemic administration both in terms of efficacy and safety. Upon induction, IFN- α was specifically released in the TME, leaving tumor-free tissues and distal organs unaffected, whereas recombinant IFN- α treatment induced IFN gene signature in a broad set of tissues. Moreover, systemic treatment of GBM-bearing mice resulted in early tumor growth inhibition that was lost overtime and associated with a lack of survival benefit. Therefore, we envision that sustained secretion of the cytokine from tumor-infiltrating cells could not only overcome the limits of local distribution from the systemic circulation but also blunt the “peak and trough” pharmacokinetics of exogenous administration. Large fluctuations in cytokine concentration may

Fig. 8. Development and application of inducible IL-12 gene therapy strategy.

(A) Kaplan-Meier survival curves of lethally irradiated C57Bl/6 mice transplanted with HSCs transduced with either Tie2-GFP-mirT or Tie2-*Il12*-mirT ($n = 10$ mice per group) ($****P < 0.0001$, $\chi^2 = 21.03$, $df = 1$, log-rank Mantel-Cox test). **(B)** LVs containing IL-12, DHFR-IL-12, or IL-12-DHFR were used to transduce bEnd.3 cells. Cells were treated or not with TMP and supernatant collected 24 hours after TMP induction. IL-12 was measured in the supernatant by ELISA (median of 10 replicates + range for IL-12 and DHFR-IL-12 and median of 3 replicates + range for IL-12-DHFR). Values are expressed in picograms per milliliter normalized on the VCN. **(C)** Induction of IFN- γ in the supernatant of primary mouse splenocytes treated with increasing doses of IL-12, DHFR-IL-12, and IL-12-DHFR. IFN- γ was measured by ELISA (picograms per milliliter). Lines represent the estimated trend of the specific activity obtained from an asymptotic NLME model (see Materials and Methods). The dots represent five biological replicates for each dose. In the analysis, few observations were excluded since identified as outliers for the model: one for IL-12 and one for DHFR-IL-12. **(D)** VCN measured in the blood cells of CTRL ($n = 10$), IFN- α -DHFR ($n = 10$), and DHFR-IL-12 ($n = 9$) gene therapy mice after hematopoietic reconstitution. **(E)** WBC in the same mice as (D) measured at reconstitution (PRE), after the first TMP dose (7 days, intraperitoneal, 60 mg/kg daily) and 25 days after mGB2 cells injection. **(F)** ELISA performed in the same mice as (D) of IL-12 (serum) and **(G)** IFN- α (plasma). Yellow box, LLOQ of the assay. **(H)** Tumor burden (median), calculated by MRI, 33 days and 49 days after tumor injection (post hoc analysis performed only at 49 days: IFN- α -DHFR versus CTRL, $*P = 0.0183$; DHFR-IL-12 versus CTRL, $P = 0.4754$, not significant; IFN- α -DHFR versus DHFR-IL-12, $P = 0.6242$, not significant; LME model described in Materials and Methods). **(I)** Kaplan-Meier survival curves of mGB2-bearing CTRL ($n = 10$), IFN- α -DHFR ($n = 10$), and DHFR-IL-12 ($n = 9$) mice (IFN- α -DHFR versus CTRL, $**P = 0.0036$, $\chi^2 = 9.767$, $df = 1$; DHFR-IL-12 versus CTRL, $*P = 0.0432$, $\chi^2 = 5.275$, $df = 1$; log-rank Mantel-Cox test with Bonferroni correction). One mouse in the DHFR-IL-12 group survived long term even in the absence of TMP. **(J)** Serial MRI scans of the long-term survivor (DHFR-IL-12). Dashed lines show extent of tumor lesion; white arrows highlight the disappearance of the tumor over time. The horizontal red line indicates TMP treatment; black line indicates TMP removal. The long-term surviving mouse received tumor rechallenge in the contralateral brain hemisphere at day 110 after the first tumor injection.



Downloaded from https://www.science.org at Universita Vita Salute - Hospital s. Raffaele on July 14, 2022

span from subtherapeutic to potentially toxic, leading to counter-regulatory responses limiting efficacy (42).

The post-translational control of the switch gives the possibility to rapidly and reversibly turn OFF its expression upon tumor eradication or emergence of severe untoward effects without relying on more complex engineering strategies and/or irreversible elimination of transduced cells (18, 43). A marked example was that of IL-12, which caused high toxicity during hematopoietic recovery but not after full reconstitution, thus requiring tight temporal control on delivery. This finding is consistent with clinical experience with IL-12 that was accompanied by severe toxicity and highlighted the need for more sophisticated delivery strategies (9, 12). Among them, an on-demand, ligand-inducible IL-12 delivery approach based on adenoviral vector has been recently tested in a phase 1 clinical trial for patients with GBM. The results not only confirmed the anticancer potential of IL-12 for GBM treatment but also remarked the requirement for fine regulation of IL-12 expression to mitigate systemic side effects, even in the case of tumor-targeted delivery strategies (44). In this regard, our DD-based platform allowed to fully capture the anti-tumor potential of IL-12 without evident toxicities in a GBM pre-clinical model. Although further studies are necessary to detail the molecular mechanisms involved in the antitumor effects of IL-12, the occurrence of GBM clearance and the resistance to tumor re-challenge in the absence of TMP in one treated mouse support the potential for induction of adaptive immunity.

A potential caveat of our strategy comes from the bacterial origin of the DHFR-DD, which may raise concerns about its potential immunogenicity. Although we did not observe any evidence of transduced cell clearance in our experimental conditions, future clinical translation of the platform may benefit from the development of fully humanized DD controlled by clinically approved drugs. Other limitations of our study pertain to its performance only in mouse GBM models, although mGB2 tumors closely reproduce key features of human GBM.

The IFN- α fusion protein had reduced specific activity in inducing ISGs as compared to its native counterpart. This might be due to the steric hindrance afforded by the DD, which can limit the diffusion rate of the molecule and/or oligomerization of its receptors on target cell membranes. The decreased specific activity of the fusion molecule did not compromise the therapeutic benefit as compared to the use of the wt transgene. This might indicate that effective immune activation can be elicited at the tumor site once a signaling threshold has been reached and that this threshold was met and likely surpassed by the transduced cell doses used in our study. Further fusion protein improvements might be investigated to increase the functionality of the transgene, including proteolytic release and flexible linkers.

The experimental design makes it difficult to distinguish a contribution of prophylactic compared to therapeutic effects of our gene therapy strategy when using the wt molecule. The time required to achieve hematopoietic reconstitution and the confounding effect of the conditioning regimen on the tumor hinder transplanting mice with engineered HSCs after tumor challenge. Transplanting HSCs before tumor challenge, however, may mimic an adjuvant treatment where surgical resection of the primary tumor precedes administration of the transduced HSCs. The similar efficacy achieved by the wt and inducible platform, when the latter was switched ON after tumor engraftment, rules out a dependence of the benefit from transgenic IFN- α expression in tissues or plasma before tumor challenge and

indicates robust activity against established tumors. The absence of antitumor effects in the GL261 GBM model, where TEMs are absent, whereas IFN- α is detectable in the plasma before tumor injection, corroborates this hypothesis and confirms the crucial role of TEM-based delivery for anticancer response. Exposure to low cytokine concentrations occurs with our constitutive and even inducible platform in the ON state, potentially affecting hematopoietic output above certain transduction doses. Overall, our data provide a potential paradigm for developing next-generation cytokine therapy and addressing the long-sought goal of capturing their full therapeutic power for fighting lethal diseases such as GBM while preventing side effects of off-target exposure (9).

MATERIALS AND METHODS

Study design

The objective of this study was to develop an inducible system based on DD for TEM-mediated cytokine delivery in the TME of GBM that can be switched ON/OFF “on demand” by administration of a small drug, allowing cytokine expression in a space- and time-controlled manner. In vitro experiments were set up to find the best cytokine-DD fusion to ensure low basal activity in the OFF state and high inducibility in the ON state. In vitro experiments included at least five biological replicates (specified for each experiment in the figure legends) with some observations excluded since identified as outliers by the statistical model (see the “Statistical analysis” section). Best cytokine-DD candidates were tested in vivo for anticancer efficacy (tumor growth inhibition and mice survival) in a mouse model of GBM. In vivo efficacy experiments using IFN- α and IFN- α -DHFR were reproduced in at least three independent experiments. Statistical analyses to determine the necessary number of mice to obtain valid insights on therapeutic efficacy were based on the variability observed in preliminary experiments. We aimed to reach a minimum of five samples per group to carry out nonparametric statistical comparisons. For experiments involving the use of rIFN- α in vivo, CTRL mice were split and randomly assigned to one of the two groups [phosphate-buffered saline (PBS)- or rIFN- α -treated].

In in vivo experiments, where mice of the same group were treated differently (IFN- α -DHFR ON compared to OFF), randomization was performed on the basis of VCN in the PB and IFN- α plasma concentration at the time of hematopoietic reconstitution. Specific procedures like scRNA-seq, bulk RNA-seq, gene expression, and histopathological analyses were conducted only once because of the complexity and the relative abundance of replicates involved.

Blinding was not applied for objective measurements of tumor volumes performed by two different operators. For histopathological analyses, evaluation was performed by two independent pathologists in double-blind manner.

Statistical analysis

The Kaplan-Meier estimator was used to estimate survival curves, and comparisons between survival curves were performed with log-rank Mantel-Cox test. Correlations between numerical variables were evaluated with Spearman’s correlation coefficient. Numerical variables between two independent groups were evaluated with the Mann-Whitney test. Kruskal-Wallis test followed by post hoc Dunn’s analysis was performed when analyzing more than two independent groups.

Longitudinal comparisons of tumor burden (calculated by MRI) among groups were performed using a linear mixed-effects (LME) model (with random effects defined to account for repeated measures of the same mice), followed by an appropriate post hoc analysis with the R package *phia*, as described in the corresponding figure legend. In the LME model, the tumor burden was used in natural logarithmic scale to meet the assumption of normality of the residuals of the model.

The nonlinear trend of *Irf7* and *Oas1a* in cells treated with different doses of wt and inducible IFN- α was estimated with an asymptotic nonlinear mixed-effects (NLME) model with respect to the dose $\text{Asym} + (R0 - \text{Asym})e^{-\text{dose} \times \text{elrc}}$, accounting also for data coming from different experiments. The parameter *Asym* represents the horizontal asymptote (value of the plateau reached by the dependent variable). The parameter *R0* represents the intercept, and the *lrc* parameter is the natural logarithm of the rate constant. All parameters of the model were allowed to depend on the group variable. In the analysis, few observations were excluded since identified as outliers for the model (as indicated in the figure legend).

The score from the top 10 gene list of cluster 6 was obtained by (i) a linear combination of the standardized intensities of the genes with all coefficients equal to 1 and (ii) the Cox's proportional hazards model with Lasso penalty (implemented in the *glmnet* R package) on the standardized intensity of the genes to predict PFS). The parameter λ of the model was defined as the one minimizing the error obtained with a 10-fold cross-validation. In both cases, the score was then categorized with the corresponding median value obtained in the data ($>$ median versus \leq median). The ability of the categorized scores in distinguishing two groups with different risk of PFS was then assessed, estimating the corresponding Kaplan-Meier curves and testing their difference with the log-rank Mantel-Cox test.

In all post hoc analyses or, in general, when the analysis involved multiple comparisons and/or testing, the *P* values were adjusted with Bonferroni's correction. In all the analyses, two-sided tests were performed, and *P* values lower than 0.05 were considered significant. All statistical analyses were performed using R 3.5.0 (www.R-project.org/) or GraphPad Prism v.9.1.0.

SUPPLEMENTARY MATERIALS

www.science.org/doi/10.1126/scitranslmed.abl4106

Figs. S1 to S12

Tables S1 to S6

Datafile S1

MDAR Reproducibility Checklist

References (45, 46)

[View/request a protocol for this paper from Bio-protocol.](#)

REFERENCES AND NOTES

- J. T. George, H. Levine, Implications of tumor-immune coevolution on cancer evasion and optimized immunotherapy. *Trends Cancer* **7**, 373–383 (2021).
- M. E. Davis, Glioblastoma: Overview of disease and treatment. *Clin. J. Oncol. Nurs.* **20**, S2–S8 (2016).
- H. Ito, H. Nakashima, E. A. Chiocca, Molecular responses to immune checkpoint blockade in glioblastoma. *Nat. Med.* **25**, 359–361 (2019).
- C. H. June, R. S. O'Connor, O. U. Kawalekar, S. Ghassemi, M. C. Milone, CAR T cell immunotherapy for human cancer. *Science* **359**, 1361–1365 (2018).
- C. E. Brown, D. Alizadeh, R. Starr, L. Weng, J. R. Wagner, A. Naranjo, J. R. Ostberg, M. S. Blanchard, J. Kilpatrick, J. Simpson, A. Kurien, S. J. Priceman, X. Wang, T. L. Harshbarger, M. D'Apuzzo, J. A. Ressler, M. C. Jensen, M. E. Barish, M. Chen, J. Portnow, S. J. Forman, B. Badie, Regression of glioblastoma after chimeric antigen receptor T-cell therapy. *N. Engl. J. Med.* **375**, 2561–2569 (2016).
- D. A. Reardon, P. C. Gokhale, S. R. Klein, K. L. Ligon, S. J. Rodig, S. H. Ramkissoon, K. L. Jones, A. S. Conway, X. Liao, J. Zhou, P. Y. Wen, A. D. Van Den Abbeele, F. S. Hodi, L. Qin, N. E. Kohl, A. H. Sharpe, G. Dranoff, G. J. Freeman, Glioblastoma eradication following immune checkpoint blockade in an orthotopic, immunocompetent model. *Cancer Immunol. Res.* **4**, 124–135 (2016).
- M. Lim, Y. Xia, C. Bettgegowda, M. Weller, Current state of immunotherapy for glioblastoma. *Nat. Rev. Clin. Oncol.* **15**, 422–442 (2018).
- E. Gangoso, B. Southgate, L. Bradley, S. Rus, F. Galvez-Cancino, N. McGivern, E. Guc, C. A. Kapourani, A. Byron, K. M. Ferguson, N. Alfazema, G. Morrison, V. Grant, C. Blin, I. Sou, M. A. Marques-Torres, L. Conde, S. Parrinello, J. Herrero, S. Beck, S. Brandner, P. M. Brennan, P. Bertone, J. W. Pollard, S. A. Quezada, D. Sproul, M. C. Frame, A. Serrels, S. M. Pollard, Glioblastomas acquire myeloid-affiliated transcriptional programs via epigenetic immunoeediting to elicit immune evasion. *Cell* **184**, 2454–2470.e26 (2021).
- A. W. Li, W. A. Lim, Engineering cytokines and cytokine circuits. *Science* **370**, 1034–1035 (2020).
- J. M. Kirkwood, C. Bender, S. Agarwala, A. Tarhini, J. Shipe-Spotloe, B. Smelko, S. Donnelly, L. Stover, Mechanisms and management of toxicities associated with high-dose interferon alfa-2b therapy. *J. Clin. Oncol.* **20**, 3703–3718 (2002).
- B. S. Parker, J. Rautela, P. J. Hertzog, Antitumour actions of interferons: Implications for cancer therapy. *Nat. Rev. Cancer* **16**, 131–144 (2016).
- W. Lasek, R. Zagodzón, M. Jakobsiak, Interleukin 12: Still a promising candidate for tumor immunotherapy? *Cancer Immunol. Immunother.* **63**, 419–435 (2014).
- B. Gentner, I. Visigalli, H. Hiramatsu, E. Lechman, S. Ungari, A. Giustacchini, G. Schira, M. Amendola, A. Quattrini, S. Martino, A. Orlacchio, J. E. Dick, A. Biffi, L. Naldini, Identification of hematopoietic stem cell-specific miRNAs enables gene therapy of globoid cell leukodystrophy. *Sci. Transl. Med.* **2**, 58ra84 (2010).
- G. Escobar, D. Moi, A. Ranghetti, P. Ozkal-Baydin, M. L. Squadrato, A. Kajaste-Rudnitski, A. Bondanza, B. Gentner, M. De Palma, R. Mazzieri, L. Naldini, Genetic engineering of hematopoiesis for targeted IFN- α delivery inhibits breast cancer progression. *Sci. Transl. Med.* **6**, 217ra213 (2014).
- M. De Palma, R. Mazzieri, L. S. Politi, F. Pucci, E. Zonari, G. Sitia, S. Mazzoleni, D. Moi, M. A. Venneri, S. Indraco, A. Falini, L. G. Guidotti, R. Galli, L. Naldini, Tumor-targeted interferon-alpha delivery by Tie2-expressing monocytes inhibits tumor growth and metastasis. *Cancer Cell* **14**, 299–311 (2008).
- M. Catarinella, A. Monestiroli, G. Escobar, A. Flocchi, N. L. Tran, R. Aiolfi, P. Marra, A. Esposito, F. Cipriani, L. Aldrighetti, M. Iannaccone, L. Naldini, L. G. Guidotti, G. Sitia, IFN α gene/cell therapy curbs colorectal cancer colonization of the liver by acting on the hepatic microenvironment. *EMBO Mol. Med.* **8**, 155–170 (2016).
- G. Escobar, L. Barbarossa, G. Barbiera, M. Norelli, M. Genua, A. Ranghetti, T. Plati, B. Camisa, C. Brombin, D. Cittaro, A. Annoni, A. Bondanza, R. Ostuni, B. Gentner, L. Naldini, Interferon gene therapy reprograms the leukemia microenvironment inducing protective immunity to multiple tumor antigens. *Nat. Commun.* **9**, 2896 (2018).
- A. T. Das, L. Tenenbaum, B. Berkhout, Tet-on systems for doxycycline-inducible gene expression. *Curr. Gene Ther.* **16**, 156–167 (2016).
- L. A. Banaszynski, M. A. Sellmyer, C. H. Contag, T. J. Wandless, S. H. Thorne, Chemical control of protein stability and function in living mice. *Nat. Med.* **14**, 1123–1127 (2008).
- L. Quintino, G. Manfre, E. E. Wettergren, A. Namislo, C. Isaksson, C. Lundberg, Functional neuroprotection and efficient regulation of GDNF using destabilizing domains in a rodent model of Parkinson's disease. *Mol. Ther.* **21**, 2169–2180 (2013).
- E. W. Weber, K. R. Parker, E. Sotillo, R. C. Lynn, H. Anbunathan, J. Lattin, Z. Good, J. A. Belk, B. Daniel, D. Klysz, M. Malipatolla, P. Xu, M. Bashti, S. Heitzeneder, L. Labanieh, P. Vandriss, R. G. Majzner, Y. Qi, K. Sandor, L. C. Chen, S. Prabhu, A. J. Gentles, T. J. Wandless, A. T. Satpathy, H. Y. Chang, C. L. Mackall, Transient rest restores functionality in exhausted CAR-T cells through epigenetic remodeling. *Science* **372**, (2021).
- B. Costa, M. N. C. Fletcher, P. Boskovic, E. L. Ivanova, T. Eisemann, S. Lohr, L. Bunse, M. Lower, S. Burchard, A. Korshunov, N. Coltella, M. Cusimano, L. Naldini, H. K. Liu, M. Platten, B. Radlwimmer, P. Angel, H. Peterziel, A set of cell lines derived from a genetic murine glioblastoma model recapitulates molecular and morphological characteristics of human tumors. *Cancers* **13**, 230 (2021).
- A. Blank, I. Kremenskaia, R. M. Urbantag, G. Acker, K. Turkowski, J. Radke, U. C. Schneider, P. Vajkoczy, S. Brandenburg, Microglia/macrophages express alternative proangiogenic factors depending on granulocyte content in human glioblastoma. *J. Pathol.* **253**, 160–173 (2021).
- M. N. Dudley, R. E. Levitz, R. Quintiliani, J. M. Hickingbotham, C. H. Nightingale, Pharmacokinetics of trimethoprim and sulfamethoxazole in serum and cerebrospinal fluid of adult patients with normal meninges. *Antimicrob. Agents Chemother.* **26**, 811–814 (1984).
- A. C. Buzaid, A. Robertone, C. Kisala, S. E. Salmon, Phase II study of interferon alfa-2a, recombinant (Roferon-A) in metastatic renal cell carcinoma. *J. Clin. Oncol.* **5**, 1083–1089 (1987).

26. E. J. Wherry, S. J. Ha, S. M. Kaech, W. N. Haining, S. Sarkar, V. Kalia, S. Subramaniam, J. N. Blattman, D. L. Barber, R. Ahmed, Molecular signature of CD8⁺ T cell exhaustion during chronic viral infection. *Immunity* **27**, 670–684 (2007).
27. A. Le Bon, G. Schiavoni, G. D'Agostino, I. Gresser, F. Belardelli, D. F. Tough, Type I interferons potently enhance humoral immunity and can promote isotype switching by stimulating dendritic cells in vivo. *Immunity* **14**, 461–470 (2001).
28. B. Maier, A. M. Leader, S. T. Chen, N. Tung, C. Chang, J. LeBerichel, A. Chudnovskiy, S. Maskey, L. Walker, J. P. Finnigan, M. E. Kirkling, B. Reizis, S. Ghosh, N. R. D'Amore, N. Bhardwaj, C. V. Rothlin, A. Wolf, R. Flores, T. Marron, A. H. Rahman, E. Kenigsberg, B. D. Brown, M. Merad, A conserved dendritic-cell regulatory program limits antitumor immunity. *Nature* **580**, 257–262 (2020).
29. S. K. Wculek, S. C. Khouili, E. Priego, I. Heras-Murillo, D. Sancho, Metabolic control of dendritic cell functions: Digesting information. *Front. Immunol.* **10**, 775 (2019).
30. M. J. C. Jordão, R. Sankowski, S. M. Brendecke, Sagar, G. Locatelli, Y. H. Tai, T. L. Tay, E. Schramm, S. Armbruster, N. Hagemeyer, O. Groß, D. Mai, Ö. Çiçek, T. Falk, M. Kerschenssteiner, D. Grun, M. Prinz, Single-cell profiling identifies myeloid cell subsets with distinct fates during neuroinflammation. *Science* **363**, eaat7554 (2019).
31. N. Ochocka, P. Segit, K. A. Walentynowicz, K. Wojnicki, S. Cyranowski, J. Swatler, J. Mieczkowski, B. Kaminska, Single-cell RNA sequencing reveals functional heterogeneity of glioma-associated brain macrophages. *Nat. Commun.* **12**, 1151 (2021).
32. M. Molgora, E. Esaulova, W. Vermi, J. Hou, Y. Chen, J. Luo, S. Brioschi, M. Bugatti, A. S. Omodei, B. Ricci, C. Fronick, S. K. Panda, Y. Takeuchi, M. M. Gubin, R. Faccio, M. Cella, S. Gilfillan, E. R. Unanue, M. N. Artyomov, R. D. Schreiber, M. Colonna, TREM2 modulation remodels the tumor myeloid landscape enhancing anti-PD-1 immunotherapy. *Cell* **182**, 886–900.e17 (2020).
33. I. Marigo, R. Trovato, F. Hofer, V. Ingangi, G. Desantis, K. Leone, F. De Sanctis, S. Ugel, S. Cane, A. Simonelli, A. Lamolinara, M. Iezzi, M. Fassin, M. Rugge, F. Boschi, G. Borile, T. Eisenhaure, S. Sarkizova, D. Lieb, N. Hacohen, L. Azzolin, S. Piccolo, R. Lawlor, A. Scarpa, L. Carbognin, E. Bria, S. Bicciato, P. J. Murray, V. Bronte, Disabled homolog 2 controls prometastatic activity of tumor-associated macrophages. *Cancer Discov.* **10**, 1758–1773 (2020).
34. M. Orecchioni, Y. Ghosheh, A. B. Pramod, K. Ley, Macrophage polarization: Different gene signatures in M1(LPS+) vs. classically and M2(LPS-) vs. alternatively activated macrophages. *Front. Immunol.* **10**, 1084 (2019).
35. S. Goswami, T. Walle, A. E. Cornish, S. Basu, S. Anandhan, I. Fernandez, L. Vence, J. Blando, H. Zhao, S. S. Yadav, M. Ott, L. Y. Kong, A. B. Heimberger, J. de Groot, B. Sepesi, M. Overman, S. Kopetz, J. P. Allison, D. Pe'er, P. Sharma, Immune profiling of human tumors identifies CD73 as a combinatorial target in glioblastoma. *Nat. Med.* **26**, 39–46 (2020).
36. E. Traggiai, L. Chicha, L. Mazzucchelli, L. Bronz, J. C. Piffaretti, A. Lanzavecchia, M. G. Manz, Development of a human adaptive immune system in cord blood cell-transplanted mice. *Science* **304**, 104–107 (2004).
37. L. Cassetta, S. Fragkogianni, A. H. Sims, A. Swierczak, L. M. Forrester, H. Zhang, D. Y. H. Soong, T. Cotechini, P. Anur, E. Y. Lin, A. Fidanza, M. Lopez-Yrigoyen, M. R. Millar, A. Urman, Z. Ai, P. T. Spellman, E. S. Hwang, J. M. Dixon, L. Wiechmann, L. M. Coussens, H. O. Smith, J. W. Pollard, Human tumor-associated macrophage and monocyte transcriptional landscapes reveal cancer-specific reprogramming, biomarkers, and therapeutic targets. *Cancer Cell* **35**, 588–602.e10 (2019).
38. K. Woroniecka, P. Chongsathidkiet, K. Rhodin, H. Kemeny, C. Dechant, S. H. Farber, A. A. Elsamadicy, X. Cui, S. Koyama, C. Jackson, L. J. Hansen, T. M. Johanns, L. Sanchez-Perez, V. Chandramohan, Y. A. Yu, D. D. Bigner, A. Giles, P. Healy, G. Dranoff, K. J. Weinhold, G. P. Dunn, P. E. Fecci, T-cell exhaustion signatures vary with tumor type and are severe in glioblastoma. *Clin. Cancer Res.* **24**, 4175–4186 (2018).
39. J. Y. Shi, Q. Gao, Z. C. Wang, J. Zhou, X. Y. Wang, Z. H. Min, Y. H. Shi, G. M. Shi, Z. B. Ding, A. W. Ke, Z. Dai, S. J. Qiu, K. Song, J. Fan, Margin-infiltrating CD20⁺ B cells display an atypical memory phenotype and correlate with favorable prognosis in hepatocellular carcinoma. *Clin. Cancer Res.* **19**, 5994–6005 (2013).
40. F. Klemm, R. R. Maas, R. L. Bowman, M. Kornete, K. Soukup, S. Nassiri, J. P. Brouland, C. A. Iacobuzio-Donahue, C. Brennan, V. Tabar, P. H. Gutin, R. T. Daniel, M. E. Hegi, J. A. Joyce, Interrogation of the microenvironmental landscape in brain tumors reveals disease-specific alterations of immune cells. *Cell* **181**, 1643–1660.e17 (2020).
41. S. Spranger, D. Dai, B. Horton, T. F. Gajewski, Tumor-residing Batf3 dendritic cells are required for effector T cell trafficking and adoptive T cell therapy. *Cancer Cell* **31**, 711–723.e4 (2017).
42. T. Clackson, Regulated gene expression systems. *Gene Ther.* **7**, 120–125 (2000).
43. V. Marin, E. Cribioli, B. Philip, S. Tettamanti, I. Pizzitola, A. Biondi, E. Biagi, M. Pule, Comparison of different suicide-gene strategies for the safety improvement of genetically manipulated T cells. *Hum. Gene Ther. Methods* **23**, 376–386 (2012).
44. E. A. Chiocca, J. S. Yu, R. V. Lukas, I. H. Solomon, K. L. Ligon, H. Nakashima, D. A. Triggs, D. A. Reardon, P. Wen, B. M. Stopa, A. Naik, J. Rudnick, J. L. Hu, P. Kumthekar, B. Yamini, J. Y. Buck, N. Demars, J. A. Barrett, A. B. Gelb, J. Zhou, F. Lebel, L. J. N. Cooper, Regulatable interleukin-12 gene therapy in patients with recurrent high-grade glioma: Results of a phase 1 trial. *Sci. Transl. Med.* **11**, eaaw5680 (2019).
45. M. De Palma, L. Naldini, Transduction of a gene expression cassette using advanced generation lentiviral vectors. *Methods Enzymol.* **346**, 514–529 (2002).
46. G. J. Lieschke, P. K. Rao, M. K. Gately, R. C. Mulligan, Bioactive murine and human interleukin-12 fusion proteins which retain antitumor activity in vivo. *Nat. Biotechnol.* **15**, 35–40 (1997).

Acknowledgments: We thank all members of Naldini's laboratory for discussion, the IRCCS San Raffaele Hospital Flow Cytometry facility (FRACAL), the IRCCS San Raffaele Center for Omics Sciences (COSR), and the IRCCS San Raffaele Hospital Advanced Light and Electron Microscopy Biologging Center (ALEMBIC). We thank T. Plati for technical support in ddPCR analyses, L. Sergi for technical help, T. Di Tomaso and A. Rigatelli for cloning IL-12, G. Escobar and L. Barbarossa for contribution to initial experiments, and C. Di Serio for coordinating CUSBS support. We also thank D. A. Reardon (Dana-Farber Cancer Institute) for GL261-Luc and P. Ghia and J. Bordini (IRCCS San Raffaele Hospital) for Rag 2^{-/-} γ chain^{-/-} mice. We also want to thank M. De Palma (EPFL) and L. Trusolino (Candiolo Cancer Institute) for critical reading of this manuscript. **Funding:** This work was supported by grants to L.N. from the Italian Association for Cancer Research (AIRC; IG 20309) and from the Louis-Jeantet Foundation through the 2019 Jeantet-Collen Prize for Translational Medicine and by European Research Council (ERC) Starting Grant 759532 (X-TAM) to R.O. F.B. and F.R. conducted this study as partial fulfillment of their PhD in Molecular Medicine, International PhD School, Vita-Salute San Raffaele University. **Author contributions:** F.B. and N.C. performed research, interpreted data, and wrote the manuscript. F.R. and M. Cusimano contributed to research and interpreted data. S.B. and I.M. performed bioinformatic analyses. L.C. and T.C. performed MRI scans. A.S. performed in vivo bioluminescence analyses. M.G. and R.O. contributed to scRNA-seq. B.C. and P.A. provided the mGB2 model and suggestions on its handling. S.C. and A.R. provided technical help. F.S., M. Callea, and R.N. performed histopathology analyses. P.M.V.R. performed statistical analyses. N.C. and L.N. designed the study, interpreted data, supervised research, and wrote the manuscript. L.N. coordinated the work. All authors have read the manuscript and agree to all its contents. **Competing interests:** L.N. is an inventor on patents on miRNA-regulated LV technology filed by the San Raffaele Scientific Institute and the Telethon Foundation. L.N. is a founder, owns equity, and chairs the scientific advisory board of Genenta Science (Nasdaq GNTA), a biotechnology company that licensed TEM-mediated IFN gene therapy and develops its clinical application. All other authors declare that they have no competing interests. **Data and materials availability:** All data associated with this study are present in the paper or the Supplementary Materials. Sequencing data are available in the Gene Expression Omnibus with the access code GSE197762: bulk RNA-seq (GSE197761) and scRNA-seq (GSE173645). Analysis results on single-cell datasets are also available at www.bioinfotiget.it/gbm/. The software used for the analyses of sequencing data is freely available at www.bioinfotiget.it/gitlab/custom/biocchi_scitramed2022. Materials can be made available upon signing a material transfer agreement with standard provisions. Some restrictions may apply on the use of the provided materials in research involving Tie2-IFN-α gene therapy, except for research aimed at reproducing the findings reported in the manuscript, according to a licensing agreement with Genenta Science.

Submitted 14 July 2021
 Accepted 19 May 2022
 Published 13 July 2022
 10.1126/scitranslmed.abl4106

Targeted inducible delivery of immunoactivating cytokines reprograms glioblastoma microenvironment and inhibits growth in mouse models

Filippo BirocchiMelania CusimanoFederico RossariStefano BerettaPaola M. V. RancoitaAnna RanghettiStefano ColomboBarbara CostaPeter AngelFrancesca SanvitoMarcella CalleaRossana NorataLinda ChaabaneTamara CanuAntonello SpinelliMarco GenuaRenato Ostunilvan MerelliNadia ColtellaLuigi Naldini

Sci. Transl. Med., 14 (653), eabl4106. • DOI: 10.1126/scitranslmed.abl4106

Controlling cytokine delivery

The immunosuppressive nature of the tumor microenvironment (TME) in glioblastoma (GBM) hinders the development of effective tumor-eradicating immunotherapies. To overcome this obstacle, Birocchi *et al.* now engineered hematopoietic stem cells (HSCs) to release of IFN- γ or IL-12 via an inducible system. In a mouse model of GBM, after HSC transplant, triggered cytokine release promoted immune cell activation in the TME. The treatment inhibited tumor growth and improved survival. The inducible HSC-mediated treatment was more effective and safer than systemic cytokine administration, suggesting that spatial and temporal precision are key factors in determining the therapeutic effects of the approach.

View the article online

<https://www.science.org/doi/10.1126/scitranslmed.abl4106>

Permissions

<https://www.science.org/help/reprints-and-permissions>

Use of this article is subject to the [Terms of service](#)